NACA RM H57G09

NACA

RESEARCH MEMORANDUM

EFFECTS OF JET EXHAUSTS ON FLIGHT-DETERMINED LONGITUDINAL AND LATERAL DYNAMIC STABILITY CHARACTERISTICS OF THE DOUGLAS D-558-II RESEARCH AIRPLANE

By Chester H. Wolowicz and Herman A. Rediess

High-Speed Flight Station
Edwards, Calif.

NATIONAL ADVISORY COMMITTEE FOR AERONAUTICS

WASHINGTON
August 23, 1957
Declassified December 1, 1959

NATIONAL ADVISORY COMMITTEE FOR AERONAUTICS

RESEARCH MEMORANDUM

EFFECTS OF JET EXHAUSTS ON FLIGHT-DETERMINED LONGITUDINAL AND LATERAL DYNAMIC STABILITY CHARACTERISTICS OF THE DOUGLAS D-558-II RESEARCH AIRPLANE

By Chester H. Wolowicz and Herman A. Rediess

SUMMARY

A flight investigation using pulse techniques has been made to determine longitudinal and lateral dynamic stability characteristics of the D-558-II research airplane with particular reference to the jet exhaust effects of the rocket engine.

Any cylinder firing combination tested that included the top cylinder resulted in a comparable loss in directional stability. These effects were most severe at the highest test Mach number of approximately 1.6. With only the two middle cylinders firing (horizontal plane), the power effects were small. At the higher supersonic Mach numbers the large adverse power effects on directional stability were insensitive to pressure ratio from 4.4 to 15.2 in the Mach number range from 1.35 to 1.56.

The power effects cause the rudder to float into the relative wind during power-on yawed flight and, as a result, tend to offset the destabilizing influence of the jet exhausts evidenced during rudder-fixed, yawed flight.

The results show that the longitudinal stability of the airplane is not influenced by the jet exhausts, probably because the horizontal tail is outside the field of action of the jet exhaust effects.

INTRODUCTION

During the early phases of the stability and control flight test investigations of the Douglas D-558-II research airplane, it was discovered that the jet exhausts of the rocket engine had an influence on the

rudder hinge moments at supersonic Mach numbers (ref. 1). A general experimental study of this influence (ref. 2) concluded that existing strong external shock waves at the jet exit during power-on conditions caused asymmetric flow fields at the rear of the vertical stabilizer. The results of a subsequent wind-tunnel investigation of the effects of a cold-jet exhaust upon the flow over the vertical stabilizer of the D-558-II airplane model at several supersonic Mach numbers showed a small influence on the lateral stability derivatives C_{Y_β}, C_{n_β}, and C_{l_β} (ref. 3). The behavior of the actual airplane, however, suggested the possibility of more pronounced power effects. As a result, particular emphasis was placed on the power effects in the flight investigation to determine the significance of this influence on the airplane's stability.

This paper presents the results of the aforementioned flight investigation. Emphasis is placed on the effect of jet exhaust on the longitudinal and lateral stability characteristics of the airplane over a Mach number range from 0.67 to 1.61. The supersonic longitudinal and lateral data and the subsonic lateral data were obtained with the D-558-II (144) rocket-powered airplane. Because of relatively little subsonic longitudinal test data available for this airplane, the data from the D-558-II (145) airplane - powered with a turbojet engine as well as a rocket engine - were used to provide a more complete coverage of the Mach number range. The data were obtained at altitudes of 20,000, 30,000, 45,000, and 60,000 feet at a nominal 1 g load factor.

The lateral flight-determined power-off stability derivatives are compared with available wind-tunnel derivatives in the appendix. In addition, the lateral derivatives are also compared with calculated derivatives.

SYMBOLS AND COEFFICIENTS

The results of this investigation are referred to the body system of orthogonal axes.

a_n	normal acceleration, g units
a_t	corrected transverse acceleration, g units
a_{t_1}	indicated transverse acceleration uncorrected for instrument position, g units
b	wing span, ft
C_{h_r}	rudder hinge-moment coefficient, $\frac{\text{Hinge moment}}{2\bar{q}Mr}$

$C_{h_{r_\beta}}$ rudder hinge-moment parameter, $\frac{\partial C_{h_r}}{\partial \beta}$

C_L lift coefficient, $\frac{\text{Lift}}{\bar{q}S}$

C_{L_0} lift coefficient for trim 1 g flight, $\frac{W}{\bar{q}S}$

C_{L_α} lift-curve slope, $\frac{\partial C_L}{\partial \alpha}$, per deg

C_l rolling-moment coefficient, $\frac{\text{Rolling moment}}{\bar{q}Sb}$

C_{l_p} damping-in-roll derivative, $\frac{\partial C_l}{\partial \frac{pb}{2V}}$, per radian

C_{l_r} rate of change of rolling-moment coefficient with yawing angular velocity factor, $\frac{\partial C_l}{\partial \frac{rb}{2V}}$, per radian

C_{l_β} effective dihedral derivative, $\frac{\partial C_l}{\partial \beta}$, per radian

C_m pitching-moment coefficient, $\frac{\text{Pitching moment}}{\bar{q}S\bar{c}}$

$C_{m_q} = \frac{\partial C_m}{\partial \frac{q\bar{c}}{2V}}$, per radian

C_{m_α} longitudinal stability derivative, $\frac{\partial C_m}{\partial \alpha}$, per deg

$C_{m_{\dot{\alpha}}} = \frac{\partial C_m}{\partial \frac{\dot{\alpha}\bar{c}}{2V}}$, per radian

C_n yawing-moment coefficient, $\frac{\text{Yawing moment}}{\bar{q}Sb}$

C_{n_p} rate of change of yawing-moment coefficient with rolling angular velocity factor, $\frac{\partial C_n}{\partial \frac{pb}{2V}}$, per radian

C_{n_r} rate of change of yawing-moment coefficient with yawing angular velocity factor, $\frac{\partial C_n}{\partial \frac{rb}{2V}}$, per radian

C_{n_β} directional stability derivatives, $\frac{\partial C_n}{\partial \beta}$, per radian

$C_{n_{\dot{\beta}}}$ rate of change of yawing-moment coefficient with rate of change of angle-of-sideslip factor, $\frac{\partial C_n}{\partial \frac{\dot{\beta} b}{2V}}$, per radian

C_Y lateral-force coefficient, $\frac{\text{Lateral force}}{\bar{q}S}$

C_{Y_β} lateral-force derivative, $\frac{\partial C_Y}{\partial \beta}$, per radian

$C_{1/2}$ number cycles to damp to one-half amplitude

$\bar{c}$ mean aerodynamic chord, ft

F_r rudder pedal force, lb

g acceleration of gravity, ft/sec^2

h_p pressure altitude, ft

I_X moment of inertia of airplane about body X-axis, $I_{X_0} \cos^2\epsilon + I_{Z_0} \sin^2\epsilon$, slug-ft^2

I_Y moment of inertia of airplane about body Y-axis, slug-ft^2

I_{XZ} product of inertia referred to body X- and Z-axes, $\frac{1}{2}\left(I_{Z_0} - I_{X_0}\right)\sin 2\epsilon$, slug-ft^2

I_Z moment of inertia of airplane about body Z-axis, $I_{Z_0} \cos^2\epsilon + I_{X_0} \sin^2\epsilon$, slug-ft^2

I_{X_0}, I_{Z_0} moments of inertia of airplane about principal longitudinal and vertical axes, respectively, slug-ft^2

M Mach number

M_r	area-moment of the rudder about the hinge line
m	mass of airplane, W/g, slugs
P	period of damped natural frequency of airplane, sec
p'	rolling angular velocity factor, $\frac{pb}{2V}$, radians
p_e	nozzle exit pressure, lb/sq ft, abs
p_o	static pressure, lb/sq ft
$\bar{q}$	dynamic pressure, $\frac{1}{2}\rho V^2$, lb/sq ft
$p,q,r,\dot{\alpha},\dot{\beta}$	rate of change with time of φ, θ, ψ, α, and β, respectively, radians/sec
$\dot{p},\dot{q},\dot{r}$	rate of change with time of p, q, and r, respectively, radians/sec^2
r'	yawing angular velocity factor, $\frac{rb}{2V}$, radians
r_1	indicated yawing angular velocity, radians
$\dot{r}_1$	indicated yawing acceleration, radians/sec^2
S	wing area, sq ft
$T_{1/2}$	time required for absolute value of transient oscillation to damp to half amplitude, sec
t	time, sec
V	airspeed, ft/sec
v	side velocity, $\frac{\beta V}{57.3}$, ft/sec
v_e	equivalent side velocity, $(v\sqrt{\sigma})$, ft/sec
W	weight of airplane, lb
X_{a_t}	distance from center of gravity to transverse accelerometer (measured parallel to body X-axis), positive when forward of center of gravity, ft
X_β	distance from center of gravity to sideslip vane (measured parallel to body X-axis), positive when forward of center of gravity, ft

Z_{a_t} distance from center of gravity to transverse accelerometer (measured perpendicular to body X-axis), positive when below center of gravity, ft

α angle of attack of airplane, deg

α_0 trim angle of attack for 1 g, deg

β corrected angle of sideslip, deg or radians

β_1 indicated angle of sideslip, radians

δ_{a_t} total aileron deflection, positive when left aileron deflected down, deg

δ_e elevator deflection, positive when elevator deflected down, deg

δ_r rudder deflection, positive when rudder deflected to left, deg

ϵ angle between referenced body X-axis and principal X-axis, positive when reference axis is above principal axis at the nose, deg

ζ ratio of actual damping to critical damping

θ angle of pitch, positive when airplane nose pitches up, radians

ρ mass density of air, slugs/cu ft

σ air-density ratio

τ time conversion parameter, $m/\rho VS$, sec

Φ phase angle, deg

Φ_d damping angle, deg

φ angle of roll, positive when right wing moves down, radians

ψ angle of yaw, positive when airplane turns to right, radians

The symbol $|j|$ represents the absolute magnitude of a j quantity and is positive. When employed in an equation, the equation is considered to be a vector equation.

The phase angle of a vector j relative to another vector k is indicated by the subscripts in Φ_{jk}. The second subscript k is used as the reference.

AIRPLANE

The D-558-II research airplane (figs. 1 and 2) is a midwing airplane with a 35° swept wing and 40° swept tail surfaces as measured at 30 percent of the mean aerodynamic chord. It is equipped with plain flap-type unboosted control surfaces linked directly to the control wheel and rudder pedals. The D-558-II (145) airplane used for subsonic and transonic investigations is powered by a J34-WE-40 turbojet engine and an LR8-RM-6 rocket engine. The D-558-II (144) airplane used primarily for supersonic investigations is powered solely by an LR8-RM-6 rocket engine.

In the D-558-II (145) airplane the turbojet engine exhausts out the bottom of the fuselage between the wing and the tail at an angle of approximately 8° relative to the body X-axis. The airplane is powered by only the turbojet engine at Mach numbers below 0.85. At Mach numbers above 0.85, it is powered by both the turbojet and the rocket engines.

The rocket engine in both airplanes has four nozzles which exhaust out the rear of the fuselage, with the thrust line of the combined nozzles coincident with the fuselage center line. These nozzles may be fired in any desired combinations. For some of the test flights the all-rocket airplane was equipped with nozzle extensions designed to expand the exhaust gases to ambient pressure at 28,000 feet. Figure 3 is a photograph of these nozzle extensions.

The physical characteristics of the D-558-II airplane are presented in table I.

The weight of the airplane at the time of the pulse maneuvers was between 10,000 and 12,000 pounds. The centers of gravity and moments of inertia for these weight values are listed in table II.

The values of I_Y were determined by adding the analytically determined contributions of the fuel to the empty weight values of I_Y determined by ground-conducted oscillation techniques. The rather uncertain values of I_X determined by ground-conducted oscillations made it advisable to use the manufacturer's estimate of I_X for the design weight

condition, then analytically correct this value of I_X for fuel consumed. The value of I_Z was determined by assuming $I_Z = I_X + I_Y$.

INSTRUMENTATION AND INSTRUMENT ACCURACY

Standard NACA instruments were used to record airspeed, altitude, angular velocities and accelerations, normal acceleration, transverse acceleration, angles of attack and sideslip, and rudder, aileron, elevator, and stabilizer positions. The airspeed, altitude, and angles of attack and sideslip were sensed on the nose boom. All records were synchronized at 0.1-second intervals by a common timing circuit.

The turn meters used to measure the angular velocities and accelerations were referenced to the body system of axes of the airplane and are considered accurate to within ±1.0 percent of scale range. The pitch turn meter had 2.1° uptilt relative to the X-axis; this error in installation was not significant. The roll turn meter had 0.5° uptilt relative to the X-axis; the yaw turn meter had 1.0° uptilt relative to the X-axis and 0.5° tilt to the left relative to the Y-axis.

Indicated sideslip angles and angles of attack, measured by vane-type pickups, were corrected for roll and yaw rate, and pitch-rate effects, respectively. The pickups were magnetically damped and had dynamically flat frequency-response characteristics over the frequency range of the airplane. The pickups are statically accurate to ±0.2°.

The ranges and dynamic characteristics for the pertinent instrumentation employed are:

Function	Range	Undamped natural frequency, cps	Damping ratio
α, deg	-20 to 40	10.0	0.70
β, deg	±30.0	10.0	.70
p, radians/sec	±3.5	18.5	.67
q, radians/sec	±1.0	18.5	.65
r, radians/sec	±1.0	14.2	.63
a_n, g units	-1 to 8	16.0	.65
a_t, g units	±1.0	13.5	.65

All data employed in the analysis were corrected for instrument phase lag. Position corrections were applied by time-vector methods of analysis to indicated linear accelerometer readings.

Rudder, aileron, elevator, and stabilizer positions were measured by standard control-position transmitters linked directly to the control surfaces. The elevator position was measured referenced to the stabilizer. The transmitter-recorder system had a flat dynamic response over the frequency range of the control movements encountered and is considered accurate to within $\pm 0.1^{\circ}$.

The nose-boom installation for measuring the airspeed was calibrated by the NACA radar-phototheodolite method. The Mach numbers presented are considered accurate to ±0.01 at speeds below $M = 0.90$ and at speeds above $M = 1.04$; ±0.02 to ±0.03 in the Mach number range from 0.90 to 1.04.

TESTS

The test procedure consisted of recording the airplane response to abrupt elevator pulses in the longitudinal stability investigation and to abrupt rudder or aileron pulses in the lateral stability phase of the investigation. The maximum oscillatory sideslip was generally of the order of 3° or less for subsonic conditions and 2° or less for supersonic conditions. The difficulty of controlling the all-rocket airplane in supersonic flight (ref. 1) made the investigation of the power effects, particularly on the lateral stability of this airplane, a lengthy process of repeated flights to obtain data which could be analyzed quantitatively. Initially, the pilot found it impossible to maintain neutral rudder after making supersonic power-on rudder-pulse maneuvers. It was necessary to devise a pin and slotted sector to enable him to hold the rudder in the neutral position following the pulse. This difficulty was not evident during the power-off supersonic flight. To eliminate any inadvertent aileron motions the control wheel was locked by a chain device for the supersonic maneuvers.

The rocket engine chamber pressure was maintained at approximately 245 psi gage. The nozzle exit pressure without nozzle extensions was 1/17 of the absolute chamber pressure; with nozzle extensions the nozzle exit pressure was 1/53 of the absolute chamber pressure. The use of nozzle extensions provided a convenient means of changing the pressure ratio p_e/p_0.

ANALYSIS OF FLIGHT DATA

The longitudinal derivatives C_{L_α}, C_{m_α}, and $\left(C_{m_q} + C_{m_{\dot{\alpha}}}\right)$ were determined by using the following relations:

$$C_{L_\alpha} = C_{L_O} \frac{|a_n|}{|\alpha|} \tag{1}$$

$$C_{m_\alpha} = -\frac{I_Y}{\bar{q}S\bar{c}}\left[\left(\frac{2\pi}{P}\right)^2 + \left(\frac{0.693}{T_{1/2}}\right)^2\right] \tag{2}$$

$$\left(C_{m_q} + C_{m_{\dot{\alpha}}}\right) = \frac{4I_Y V}{\bar{q}S\bar{c}^2}\left[\frac{C_{L_\alpha}}{4\tau} - \frac{0.693}{T_{1/2}}\right] \tag{3}$$

The lateral derivatives were obtained by employing the time-vector method outlined in reference 4. The results in the present paper, however, are relative to the body axes, whereas reference 4 dealt with the stability axes. Figure 4 is a sample of the time-vector solution relative to the body axes. The use of the body axes affected the vector diagram for the side-force equation (fig. 4(c)) by introducing an additional vector $\left(-2\tau\alpha \frac{|p|}{|\beta|}\right)$.

There is considerable uncertainty regarding the inclination of the principal axis. Preliminary calculations indicated that an inclination of 1.5° down at the nose relative to the body X-axis provided reasonable correlation between flight and preliminary theoretical estimations of C_{n_r} in the supersonic range. It is believed the inclination of the principal axis thus determined is known possibly to within 0.5°. However, this magnitude of uncertainty can result in poor accuracy of $\left(C_{n_r} - C_{n_{\dot{\beta}}}\right)$ and still not appreciably affect the magnitude of C_{n_β}, C_{l_β}, and C_{l_p}. Therefore, the lateral derivatives presented in this paper do not include $\left(C_{n_r} - C_{n_{\dot{\beta}}}\right)$.

The values of C_{l_r} and C_{n_p} (fig. 5) required for the time-vector solution of the remaining derivatives were obtained from theoretical estimates.

PRESENTATION OF RESULTS

The results of the investigation are presented in two general parts: (1) the longitudinal stability characteristics, and (2) the lateral

stability characteristics. Inasmuch as particular emphasis is placed on power effects, the discussion, with the aid of figure 6, briefly reviews the mechanics of the power effects first. The pertinent results of the investigation are presented in the figures listed in the following tabulation:

	Figures
Longitudinal stability characteristics:	
Time histories of elevator-induced oscillations	7
Variation of trim C_L and trim α with Mach number	8
Period and damping characteristics	9
Longitudinal stability derivatives	10
Comparison of flight derivatives with wind-tunnel derivatives	11
Lateral stability characteristics:	
Time histories comparing power-on and power-off lateral oscillations	12
Period and damping characteristics	13
Power effects on amplitude ratios and phase angles	14, 15
Power influence on stability derivatives	16
Comparison of lateral oscillatory characteristics with lateral damping criteria	17
Time histories comparing power-on rudder-free and rudder-fixed oscillations	18
Influence of free rudder on period and damping characteristics; power on	19
Influence on stability derivatives of free rudder during powered flight	20
Approximate variation of rudder hinge-moment parameter with Mach number at different pressure ratios	21
In the appendix may be found:	
Vertical-tail areas used in estimating derivatives	22
Comparison of flight derivatives with calculated and available wind-tunnel derivatives for power-off conditions	23

DISCUSSION

Before discussing the jet exhaust effects on the stability characteristics of the airplane, it is believed pertinent to consider some of the qualitative aspects of the shock-wave behavior at the juncture of the vertical tail and fuselage due to jet streams exhausting at the rear of the fuselage. On this basis it is desirable to review the principle of the shock-wave behavior. The following discussion is based primarily on reference 2.

When a body has a jet exhausting at a sufficiently high pressure ratio into a free stream in yawed supersonic flight, the stream flow cannot turn through the deflection angle formed by the body and the outline of the jet exhaust. As a result, the boundary layer on the lee side of the body thickens and separates upstream of the jet exit (fig. 6). The external shock wave at the jet exit on the lee side of the body becomes a lambda shock with one leg forming forward in the lower pressure region and, in the absence of the vertical tail, the other leg remaining at the lip of the exit. On the upstream side of the body there is no separation of the boundary layer and a simple shock wave is present at the lip of the jet exit.

The introduction of a vertical tail (or a horizontal tail) in this unsymmetrical flow field causes the lambda shock wave to move forward into the low-pressure region of the vertical tail; the shock wave on the other side of the vertical tail remains attached to the jet exit. Inasmuch as the pressure behind the external shock wave is higher than in front of it, the forward movement of the lambda shock wave on the lee side of the vertical tail results in higher pressures on the vertical tail than would be experienced if the shock wave were not present. The result is a decrease in the stabilizing action of the vertical tail for rudder-locked conditions. If the configuration has some of the rudder surface within the field of the shock-wave action, the higher pressures behind the shock wave on the lee side of the rudder tend to turn the rudder into the free stream. With a free rudder, this shock-wave-induced turning of the rudder into the free stream provides a stabilizing action.

Longitudinal Stability Characteristics

Several time histories are presented in figure 7 and indicate no unusual longitudinal characteristics in the D-558-II airplane. The variation with Mach number of the level-flight lift coefficient C_{L_0} and trim angle of attack α_0, shown in figure 8 for the five test altitudes, indicated normal characteristics. The scatter of the C_{L_0} test data in figure 8 is attributed to weight and altitude differences. The α_0 test points have been reduced to 1 g load-factor conditions by applying the following correction:

$$\Delta\alpha = \frac{C_{L_0}(a_n - 1)}{C_{L_\alpha}}$$

The period and damping variation with Mach number and altitude (fig. 9) and the longitudinal derivatives (fig. 10) showed no power-on

jet exhaust effects for the nozzle-extension-on and nozzle-extension-off configurations which were used to obtain data for the pressure ratio (p_e/p_0) range from about 2 to 15. It appears likely that the horizontal-tail surface is located at a sufficient distance above the rocket nozzles and shock-wave formations to be out of the field of influence. Had the horizontal tail been located in the vicinity of the longitudinal reference axis of the airplane with its trailing edge close to the edge of the body, it is conceivable that power effects would be evident.

The period and damping ratio curves (fig. 9) show in general a normal variation with Mach number. Inasmuch as the derivatives shown in figure 11 do not show any altitude effects, the variations of the period and damping ratio with altitude are functions of air density for all practical purposes. Note, however, that in the Mach number range of 0.85 to 0.90 there are discontinuities which are reflected in the derivatives. The damping ratio curves (fig. 9) indicate a large decrease in damping ratio is experienced in the supersonic region. This decrease would be attributed primarily to the large negative increase in C_{m_α} in the supersonic region over the values in the subsonic region (fig. 10).

The erratic behavior of the $(C_{m_q} + C_{m_{\dot{\alpha}}})$ curve (fig. 10) in the transonic Mach number range from 0.80 to about 0.92 is shown in reference 5 to be a characteristic of wings of this type.

A comparison of flight and wind-tunnel values of C_{L_α} and C_{m_α} is presented in figure 11. The flight-determined values of the derivatives show generally good agreement with the wind-tunnel data of references 6 to 8.

Lateral Stability Characteristics

Rudder fixed.- Time histories of representative rudder-pulse maneuvers for power-on and power-off conditions with the rudder fixed during the transient portion of the maneuvers are shown in figure 12. The destabilizing influence of power on the period is very evident. In any consideration of the power effects on the airplane, the cylinders fired and the pressure ratio p_e/p_0 may be of prime importance. Although the data obtained were not of the desired quantity, they did provide a good insight into the effect of cylinders fired and the influence of pressure ratios on the stability. It should be kept in mind that the following results of the present investigation are based on data wherein the maximum supersonic oscillatory sideslip angle was of the order of 2° or less. References 2 and 3 point out that the magnitude of the jet exhaust effects (for rudder-free as well as rudder-fixed conditions) is influenced by the magnitude of the sideslip angle as well as pressure ratio and Mach number.

A study of the period curves in figure 13 for an altitude of approximately 60,000 feet shows that when number 1 cylinder was firing, there was no appreciable change in the period when the pressure ratio was increased from 4.7 to 15.2 at $M = 1.4$ and from 4.4 to 13 in the vicinity of $M = 1.5$. When number 1 cylinder was eliminated from the firing combinations as at a Mach number of 1.49 and 1.58 (refer to period plot in fig. 13), the destabilizing influence of power decreased very markedly. Since the number 1 cylinder is in a dominant position for power effects (fig. 3), it would be the first cylinder to bring about a flow separation on the lee side of the vertical tail. Conversely, it would generally be supposed that a change in pressure ratio from about 4.5 to about 14 would result in larger destabilizing influences than those shown. Had high pressure-ratio data been available at $M = 1.28$ for comparison with low pressure-ratio data at this Mach number, greater changes in period might have been evidenced than shown at $M = 1.4$. This conjecture is based on limited data obtained at an altitude of 45,000 feet and will be discussed in a later section.

A slightly favorable increase in $\frac{1}{T_{1/2}}$ and ζ as a result of power is indicated in the vicinity of a Mach number of 1.3 (fig. 13); however, at the high test Mach number of 1.56 the power effect appears to be detrimental.

All the amplitude ratios and phase angles (figs. 14 and 15) show power effects which increase with increasing Mach number. The reduction in $\frac{|a_t|}{|\beta|}$ resulting from power (fig. 14) signifies a corresponding reduction in C_{Y_β} (fig. 16). The increase in $\frac{|\varphi|}{|\psi|}$ which is approximately 2.5 times the power-off value of 6.7 at $M = 1.5$ is usually undesirable in regard to handling qualities.

The influence of jet exhaust effects on the lateral stability derivatives in which the number 1 cylinder was included in the firing combination is shown in figure 16. The seemingly moderate reduction in C_{Y_β} at higher supersonic Mach numbers due to the power effects is evidenced as a serious reduction in C_{n_β} and a significant reduction in C_{l_β}. For example, at $M = 1.5$ the decrease of 0.10 in C_{Y_β} due to a loss in the vertical-tail effectiveness as a result of power effects, signifies a decrease in vertical-tail contribution to C_{n_β} from 0.34 to 0.27. Inasmuch as the wing-fuselage combination provides a destabilizing contribution to C_{n_β} of about -0.19, the seemingly small loss in vertical-tail contribution is very significant.

It will be noticed that the adverse effects of the jet exhaust on the stability derivatives tend to level off with increasing supersonic Mach number. It is quite possible that the power-on and power-off characteristics of the airplane may become very similar at some higher Mach number.

No attempt is made at this time to consider the variation with Mach number of the lateral derivatives for power-off conditions. Consideration of the derivatives will be made later in sections dealing with the comparison of the derivatives with available wind-tunnel data and calculated derivatives.

As a matter of interest the Dutch roll characteristics of the airplane for power-off and power-on conditions of supersonic flight at an altitude of 60,000 feet are compared in figure 17 with appropriate phases of the damping criteria of reference 9. The figure shows that neither power condition would satisfy boundary A at this altitude; however, if the airplane were considered to be equipped with artificial stabilization devices which were temporarily inoperative, the lower boundary shown in figure 17 for this condition would have been generally satisfied at an altitude of 60,000 feet and over the Mach number range investigated. The pilot considered the airplane easy to handle during power-off supersonic flight at an altitude of 60,000 feet and, even though the addition of power resulted in some deterioration of its handling qualities, it was still controllable.

Rudder free.- As was explained in the "Tests" section, the pilot was unable to hold the rudder in a steady neutral position by using only the rudder pedals during the transient phase of a pulse maneuver in power-on supersonic flight. It was noted that this rudder-free, power-on lateral period of oscillation in the supersonic region was shorter than the rudder-locked, power-on lateral periods, thus suggesting an improvement in lateral stability during oscillatory, power-on, supersonic flight by having the rudder free. This is shown in time histories presented in figure 18.

The rudder-free, power-on data, obtained at 45,000 feet, are rather meager; however, the quality of the few data points utilized is considered to be good. The rudder-free, power-on stability characteristics based on these points are shown in figures 19 and 20. Included in these figures are several rudder-fixed points for both power conditions. Also included, for purposes of comparing trends and levels, are previously presented rudder-fixed curves for an altitude of 60,000 feet for both power conditions.

Figure 19 and the derivative plots in figure 20 show that at a Mach number of 1.41 the rudder-free, power-on stability at the low pressure ratio of 2.2 with all cylinders firing was similar to the power-off

rudder-fixed stability. This signifies an improvement in rudder-free stability due to power effects, inasmuch as figure 21 (reproduced from ref. 1) shows that the rudder tends to float with the relative wind during power-off flight at this Mach number. Thus the favorable effect of power on the rudder-free stability counteracts the adverse effect of power on rudder-fixed stability which was evident in figures 19 and 20 at a Mach number of 1.37 for the same power conditions. No rudder-free data were available for higher pressure ratios; however, on the basis of figure 21 an increase in pressure ratio for rudder-free flight conditions would have resulted in further stabilizing effects up to a Mach number above 1.6 (depending on pressure ratio), with the maximum influence occurring at a Mach number of about 1.4.

It is evident that while the power effects cause a maximum positive floating tendency of the rudder at a Mach number of about 1.4 (fig. 21), the vertical tail as a whole (rudder-fixed conditions) is still experiencing decreasing effectiveness. Although the inclination of the lambda shock wave tends to become normal to the surface at low supersonic Mach numbers, the shock wave is well to the rear and weak. As the Mach number increases to some higher value, it is believed that the observed power effects indicate that the increased strength and forward movement of the lambda shock wave more than compensate for the increased inclination of the shock wave.

It was conjectured in the section on rudder-fixed stability that a change in pressure ratio from about 4.5 to 14 would probably result in larger destabilizing influences at a lower Mach number (such as 1.28) rather than at about 1.5. This conjecture was made on the basis of the very limited rudder-fixed test points at an altitude of 45,000 feet and Mach numbers of 1.27 and 1.37 in figures 20 and 21. These test points showed that an increase in pressure ratio p_e/p_0 at $M = 1.21$ over the value at $M = 1.37$ more than offset the improvement in lateral stability which would have been obtained by not firing the number 1 cylinder at a Mach number of 1.28.

CONCLUSIONS

A flight investigation using pulse techniques has been made to determine the longitudinal and lateral stability characteristics of the D-558-II airplane with particular reference to the jet exhaust effects of the rocket engine. The oscillatory sideslip motions were generally of the order of 3° or less for subsonic tests and 2° or less for supersonic tests. The pertinent results of this investigation are summarized as follows:

1. Any cylinder firing combination tested that included the top cylinder resulted in a comparable loss in directional stability. These effects were most severe at the highest test Mach number of approximately 1.6. With only the two middle cylinders firing (horizontal plane), the power effects were small.

2. At the higher supersonic Mach numbers the large adverse power effects on directional stability were insensitive to pressure ratios varying from 4.4 to 15.2 in the Mach number range of 1.35 to 1.56.

3. Power effects cause the rudder to float into the relative wind during power-on yawed flight and, as a result, tend to offset the destabilizing influence of the jet exhausts evidenced during rudder-fixed yawed flight.

4. The longitudinal stability of the airplane is not influenced by the jet exhausts primarily because the horizontal tail appears to be out of the field of action of the jet exhaust effects.

High-Speed Flight Station,
National Advisory Committee for Aeronautics,
Edwards, Calif., June 18, 1957.

APPENDIX

COMPARISON OF FLIGHT DERIVATIVES WITH WIND-TUNNEL DATA AND CALCULATED DERIVATIVES

Preliminary comparisons of the power-off flight derivatives with the calculations of reference 10 showed rather large discrepancies at supersonic speeds. It appeared that the overprediction of C_{n_β} resulted from an excessive estimate of the tail contribution to the overall stability. Consequently, it was decided to reestimate the tail contribution using a different effective tail area for supersonic conditions from that used for subsonic conditions (fig. 22). The tail area for the supersonic calculations is in accord with the manufacturer's use of tail area for supersonic calculations for this airplane. The effective aspect ratios for the subsonic and supersonic tail areas were determined from reference 11 to be 1.53 and 1.47, respectively.

Tail-off estimates of C_{Y_β}, C_{n_β}, and C_{l_β} were based on wind-tunnel data obtained from references 10 and 12. The wing contributions to the dynamic stability derivatives were estimated from the methods of references 13 to 19. Subsonic horizontal-tail-interference effects on the static and dynamic stability derivatives were estimated from references 20 to 22. Vertical-tail contributions to the static and dynamic stability derivatives were calculated using effective aspect ratios, calculated lift-curve slopes (refs. 13 to 19), and the equations of reference 21.

A comparison of the flight derivatives with available wind-tunnel derivatives (refs. 10, 12, and 23) and calculated derivatives is shown in figure 23. Although the subsonic wind-tunnel data are for $M = 0.16$, the flight data extend to a sufficiently low Mach number of 0.67 to show the degree of correlation. The low subsonic value of the flight derivatives C_{n_β} and C_{l_p} shows good agreement with the wind-tunnel data. The low subsonic value of C_{Y_β} from flight data is of lower magnitude than tunnel data; the reason for this discrepancy has not been determined. The subsonic value of C_{l_β} from flight data at $M = 0.67$ is at an angle of attack of approximately 2.9°, indicating flight values of C_{l_β} to be of lower magnitude than wind-tunnel data (-0.108 as against -0.123 for wind tunnel).

It is quite possible that the subsonic flight values of C_{l_β} are somewhat low in magnitude when compared to wind-tunnel data. The reason

for this may lie in uncertainties in the true value of C_{l_r} and I_X, as well as limitations in the accuracy of experimental determination of $\frac{|\varphi|}{|\beta|}$. The calculated values of C_{l_r} (fig. 5) have a significant influence on the determination of C_{l_β} from flight data in the subsonic region; this may be appreciated from a study of the sample vector solution for the rolling derivatives (fig. 4(e)). If C_{l_r} had been assumed equal to zero, C_{l_β} would have been -0.113 instead of -0.106. Errors in the values of I_X or $\frac{|\varphi|}{|\beta|}$ of the order of ±5 percent would be sufficient to bring about an incremental change of about ±0.006 in the value of C_{l_β}.

At the higher supersonic Mach number of 1.61, the power-off flight derivatives show good correlation with available wind-tunnel data. Inasmuch as the tunnel data of reference 12 were based on a model equipped with the original (small) vertical tail, the correction to the C_{Y_β} and C_{n_β} data at $M = 1.61$ to account for the enlarged tail was estimated on the basis of the experimental data of reference 24.

The calculated derivatives of reference 10 and the calculated derivatives of this paper are compared with flight derivatives in figure 23. In the subsonic region both sets of calculated derivatives show good agreement with one another and with flight data for C_{n_β} and C_{l_p}; agreement with flight data is moderately poor for C_{Y_β}. For C_{l_β} the calculations of this paper show the greatest discrepancy with flight. This may be attributed in part to uncertainty of the position of the actual center of pressure of the vertical tail.

In the supersonic region, the calculated derivatives of this paper are in closer agreement with flight data for C_{Y_β}, C_{n_β}, and C_{l_β} than the extrapolation of reference 10, but in slightly poorer agreement for C_{l_p}.

REFERENCES

1. Ankenbruck, Herman O., and Wolowicz, Chester H.: Lateral Motions Encountered With the Douglas D-558-II All-Rocket Research Airplane During Exploratory Flights to a Mach Number of 2.0. NACA RM H54I27, 1954.

2. Hatch, John E., Jr., and Savelle, William M.: Some Effects of a Sonic Jet Exhaust on the Loading Over a Yawed Fin at a Mach Number of 3.03. NACA RM L52L02a, 1953.

3. Grigsby, Carl E.: An Investigation of the Effects of Jet Exhaust and Reynolds Number Upon the Flow Over the Vertical Stabilizer and Rudder of the Douglas D-558-II Research Airplane at Mach Numbers of 1.62, 1.93, and 2.41. NACA RM L54E03, 1954.

4. Wolowicz, Chester H.: Time-Vector Determined Lateral Derivatives of a Swept-Wing Fighter-Type Airplane With Three Different Vertical Tails at Mach Numbers Between 0.70 and 1.48. NACA RM H56C20, 1956.

5. Gillis, Clarence L., and Chapman, Rowe, Jr.: Summary of Pitch-Damping Derivatives of Complete Airplane and Missile Configurations as Measured in Flight at Transonic and Supersonic Speeds. NACA RM L52K20, 1953.

6. Osborne, Robert S.: High-Speed Wind-Tunnel Investigation of the Longitudinal Stability and Control Characteristics of a 1/16-Scale Model of the D-558-2 Research Airplane at High Subsonic Mach Numbers and at a Mach Number of 1.2. NACA RM L9C04, 1949.

7. Silvers, H. Norman, and King, Thomas J., Jr.: Investigation at High Subsonic Speeds of the Effects of Various Underwing External-Store Arrangements on the Aerodynamic Characteristics of a 1/16-Scale Model of the Douglas D-558-II Research Airplane. NACA RM L55D11, 1955.

8. Spearman, M. Leroy: Static Longitudinal Stability and Control Characteristics of a 1/16-Scale Model of the Douglas D-558-II Research Airplane at Mach Numbers of 1.61 and 2.01. NACA RM L53I22, 1953.

9. Anon.: Military Specification - Flying Qualities of Piloted Airplanes. MIL-F-8785 (ASG), Amendment -2, Oct. 17, 1955.

10. Queijo, M. J., and Goodman, Alex: Calculations of the Dynamic Lateral Stability Characteristics of the Douglas D-558-II Airplane in High-Speed Flight for Various Wing Loadings and Altitudes. NACA RM L50H16a, 1950.

11. Queijo, M. J., and Wolhart, Walter D.: Experimental Investigation of the Effect of Vertical-Tail Size and Length and of Fuselage Shape and Length on the Static Lateral Stability Characteristics of a Model With 45° Sweptback Wing and Tail Surfaces. NACA Rep. 1049, 1951.

12. Grant, Frederick C., and Robinson, Ross B.: Static Lateral Stability Characteristics of a 1/16-Scale Model of the Douglas D-558-II Research Airplane at Mach Numbers of 1.61 and 2.01. NACA RM L53I29a, 1953.

13. Toll, Thomas A., and Queijo, M. J.: Approximate Relations and Charts for Low-Speed Stability Derivatives of Swept Wings. NACA TN 1581, 1948.

14. Fisher, Lewis R.: Approximate Corrections for the Effects of Compressibility on the Subsonic Stability Derivatives of Swept Wings. NACA TN 1854, 1949.

15. DeYoung, John: Theoretical Antisymmetric Span Loading for Wings of Arbitrary Plan Form at Subsonic Speeds. NACA Rep. 1056, 1951. (Supersedes NACA TN 2140.)

16. Malvestuto, Frank S., Jr., Margolis, Kenneth, and Ribner, Herbert S.: Theoretical Lift and Damping in Roll at Supersonic Speeds of Thin Sweptback Tapered Wings With Streamwise Tips, Subsonic Leading Edges, and Supersonic Trailing Edges. NACA Rep. 970, 1950. (Supersedes NACA TN 1860.)

17. Jones, Arthur L., and Alksne, Alberta: A Summary of Lateral-Stability Derivatives Calculated for Wing Plan Forms in Supersonic Flow. NACA Rep. 1052, 1951.

18. Margolis, Kenneth: Theoretical Calculations of the Lateral Force and Yawing Moment Due to Rolling at Supersonic Speeds for Sweptback Tapered Wings With Streamwise Tips. Subsonic Leading Edges. NACA TN 2122, 1950.

19. Harmon, Sidney M., and Martin, John C.: Theoretical Calculations of the Lateral Force and Yawing Moment Due to Rolling at Supersonic Speeds for Sweptback Tapered Wings With Streamwise Tips. Supersonic Leading Edges. NACA TN 2156, 1950.

20. Brewer, Jack D., and Lichtenstein, Jacob H.: Effect of Horizontal Tail on Low-Speed Static Lateral Stability Characteristics of a Model Having 45° Sweptback Wing and Tail Surfaces. NACA TN 2010, 1950.

21. Letko, William, and Riley, Donald R.: Effect of an Unswept Wing on the Contribution of Unswept-Tail Configurations to the Low-Speed Static- and Rolling-Stability Derivatives of a Midwing Airplane Model. NACA TN 2175, 1950.

22. Bird, John D., Jacquet, Byron M., and Cowan, John W.: Effect of Fuselage and Tail Surfaces on Low-Speed Yawing Characteristics of a Swept-Wing Model as Determined in Curved-Flow Test Section of Langley Stability Tunnel. NACA RM L8G13, 1948.

23. Boatright, William B.: Wind-Tunnel Measurements of the Dynamic Cross Derivative $C_{l_r} - C_{l_{\dot{\beta}}}$ (Rolling Moment Due to Yawing Velocity and to Acceleration in Sideslip) of the Douglas D-558-II Airplane and Its Components at Supersonic Speeds Including Description of the Technique. NACA RM L55H16, 1955.

24. Robinson, Ross B.: Effects of Canopy, Revised Vertical Tail, and a Yaw-Damper Vane on the Aerodynamic Characteristics of a 1/16-Scale Model of the Douglas D-558-II Research Airplane at a Mach Number of 2.01. NACA RM L54F25, 1954.

TABLE I

PHYSICAL CHARACTERISTICS OF THE DOUGLAS D-558-II AIRPLANE

Wing:	
Root airfoil section (normal to 30-percent chord of unswept panel)	NACA 63-010
Tip airfoil section (normal to 30-percent chord of unswept panel)	NACA 63_1-012
Total area, sq ft	175.0
Span, ft	25.0
Mean aerodynamic chord, in.	87.301
Root chord (parallel to plane of symmetry), in.	108.51
Extended tip chord (parallel to plane of symmetry), in.	61.18
Taper ratio	0.565
Aspect ratio	3.570
Sweep at 30-percent chord of unswept panel, deg	35.0
Sweep of leading edge, deg	38.8
Incidence of fuselage center line, deg	3.0
Dihedral, deg	-3.0
Geometric twist, deg	0
Total aileron area (rearward of hinge line), sq ft	9.8
Aileron travel (each), deg	±15
Total flap area, sq ft	12.58
Flap travel, deg	50
Horizontal tail:	
Root airfoil section (normal to 30-percent chord of unswept panel)	NACA 63-010
Tip airfoil section (normal to 30-percent chord of unswept panel)	NACA 63-010
Total area, sq ft	39.9
Span, in.	143.6
Mean aerodynamic chord, in.	41.75
Root chord (parallel to plane of symmetry), in.	53.6
Extended tip chord (parallel to plane of symmetry), in.	26.8
Taper ratio	0.50
Aspect ratio	3.59
Sweep at 30-percent chord line of unswept panel, deg	40.0
Dihedral, deg	0
Elevator area, sq ft	9.4
Elevator travel, deg	
Up	25
Down	15

TABLE I.- Concluded.

PHYSICAL CHARACTERISTICS OF THE DOUGLAS D-558-II AIRPLANE

Stabilizer travel, deg		
Leading edge up		4
Leading edge down		5
Vertical tail:		
Airfoil section (normal to 30-percent chord of unswept panel)		NACA 63-010
Effective area, (area above root chord), sq ft		36.6
Height from fuselage reference line, in.		98.0
Root chord (parallel to fuselage center line), in.		146.0
Extended tip chord (parallel to fuselage center line), in.		27.0
Sweep angle at 30-percent chord of unswept panel, deg		49.0
Rudder area (rearward of hinge line), sq ft		6.15
Rudder travel, deg		±25
Fuselage:		
Length, ft		42.0
Maximum diameter, in.		60.0
Fineness ratio		8.40
Speed-retarder area, sq ft		5.25
	144	145
Powerplant:		
Turbojet	--------	J34-WE-40
Rocket	LR8-RM-6	LR8-RM-6
Airplane weight, lb:		
Full jet and rocket fuel	--------	15,131
Full jet fuel	--------	11,942
Full rocket fuel	15,787	--------
No fuel	9,421	10,382
Center-of-gravity locations, percent mean aerodynamic chord:		
Full jet and rocket fuel (gear up)	--------	23.5
Full jet fuel (gear up)	--------	25.2
Full rocket fuel (gear up)	24.6	--------
No fuel (gear up)	27.3	27.0
No fuel (gear down)	26.7	26.4

TABLE II

MOMENTS OF INERTIA AND CENTERS OF GRAVITY FOR NOMINALLY EXTREME FLIGHT TEST WEIGHTS OF THE AIRPLANE

Airplane	D-558-II (144)		D-558-II (145)	
Weight, lb	10,000	12,000	10,000	12,000
I_X, slug-ft^2	2,920	2,920	------	------
I_Y, slug-ft^2	33,300	36,275	31,500	34,700
I_Z, slug-ft^2	36,220	39,250	------	------
Center of gravity, percent $\bar{c}$ . . .	25	25	25	25

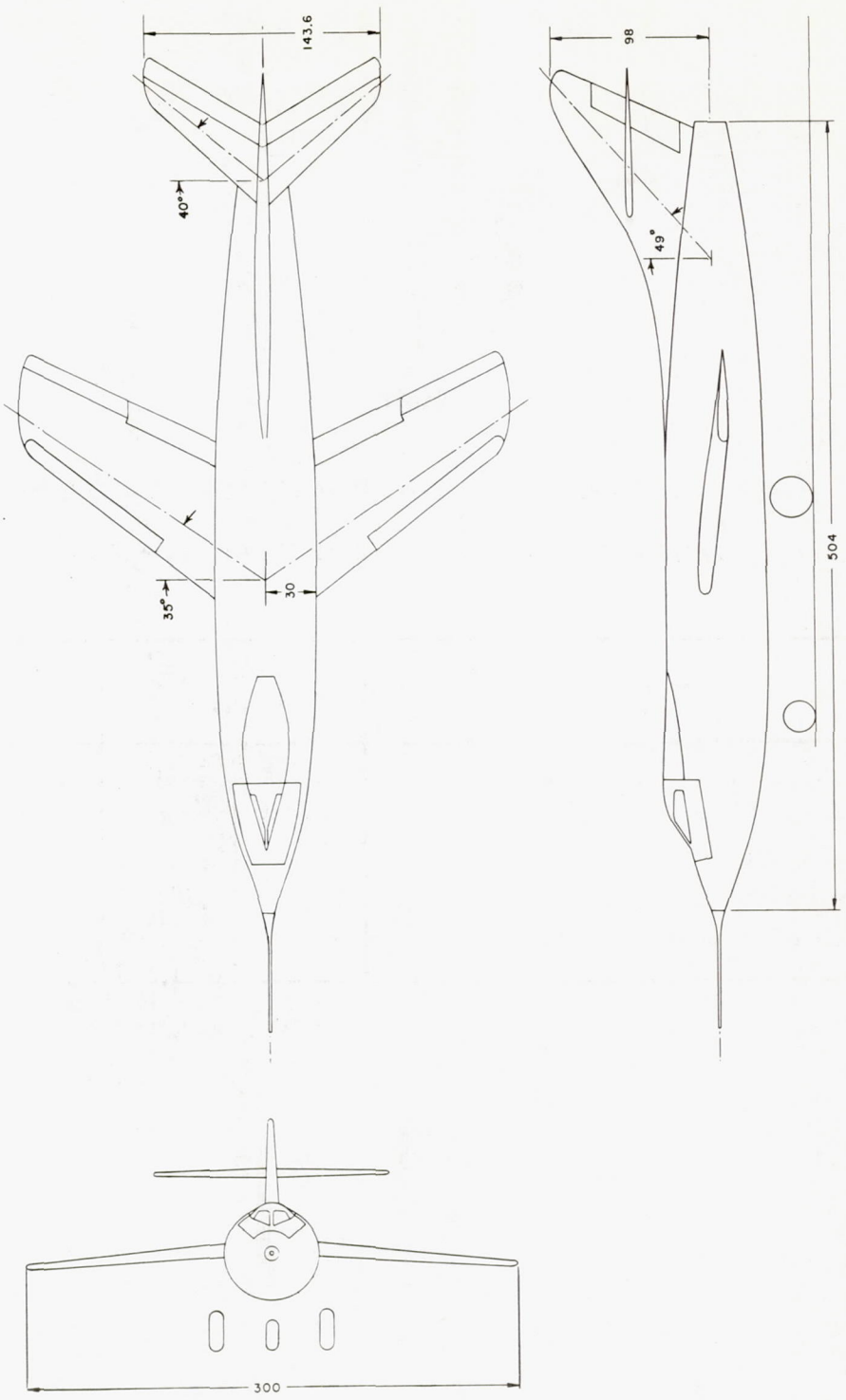
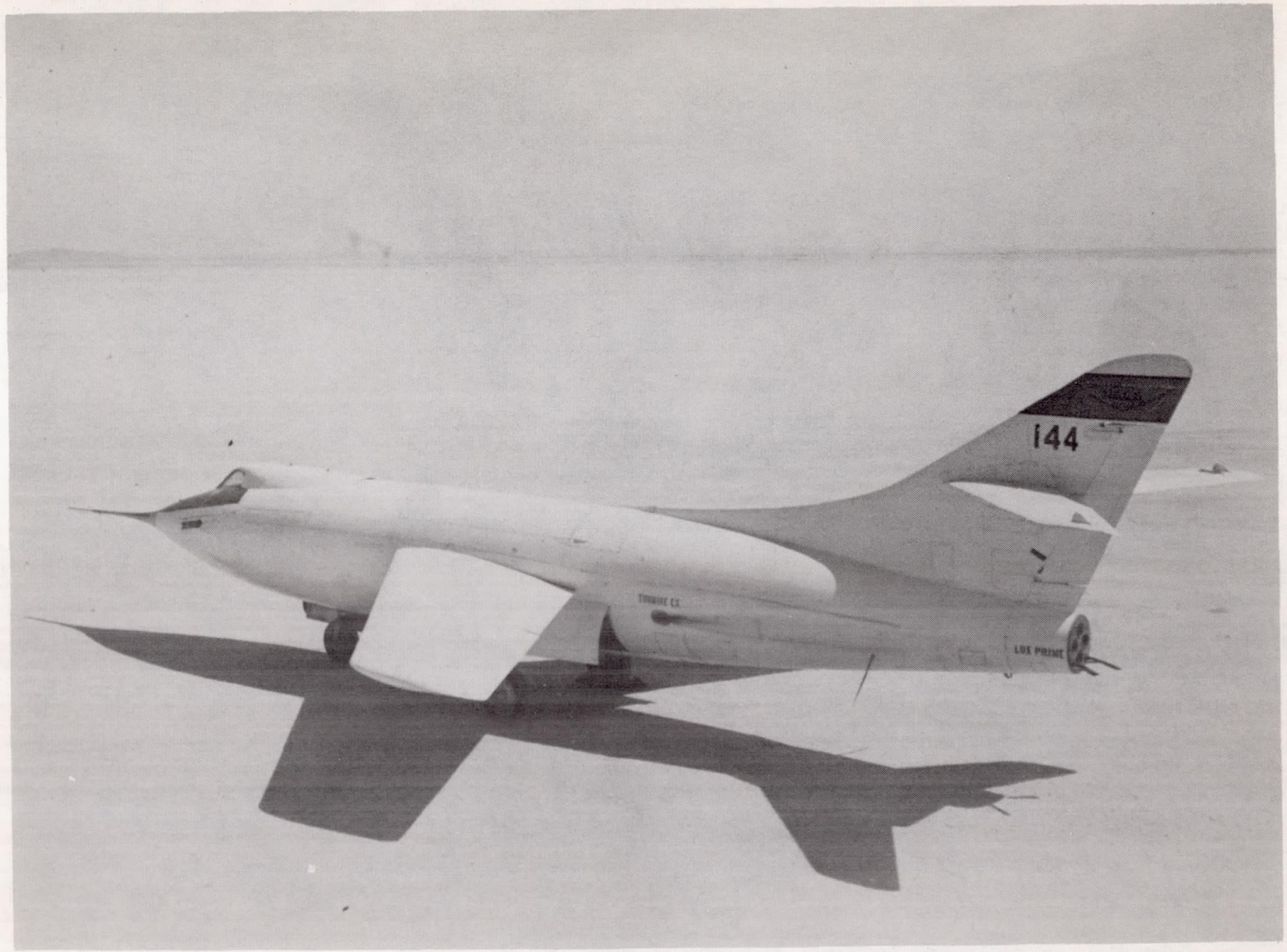
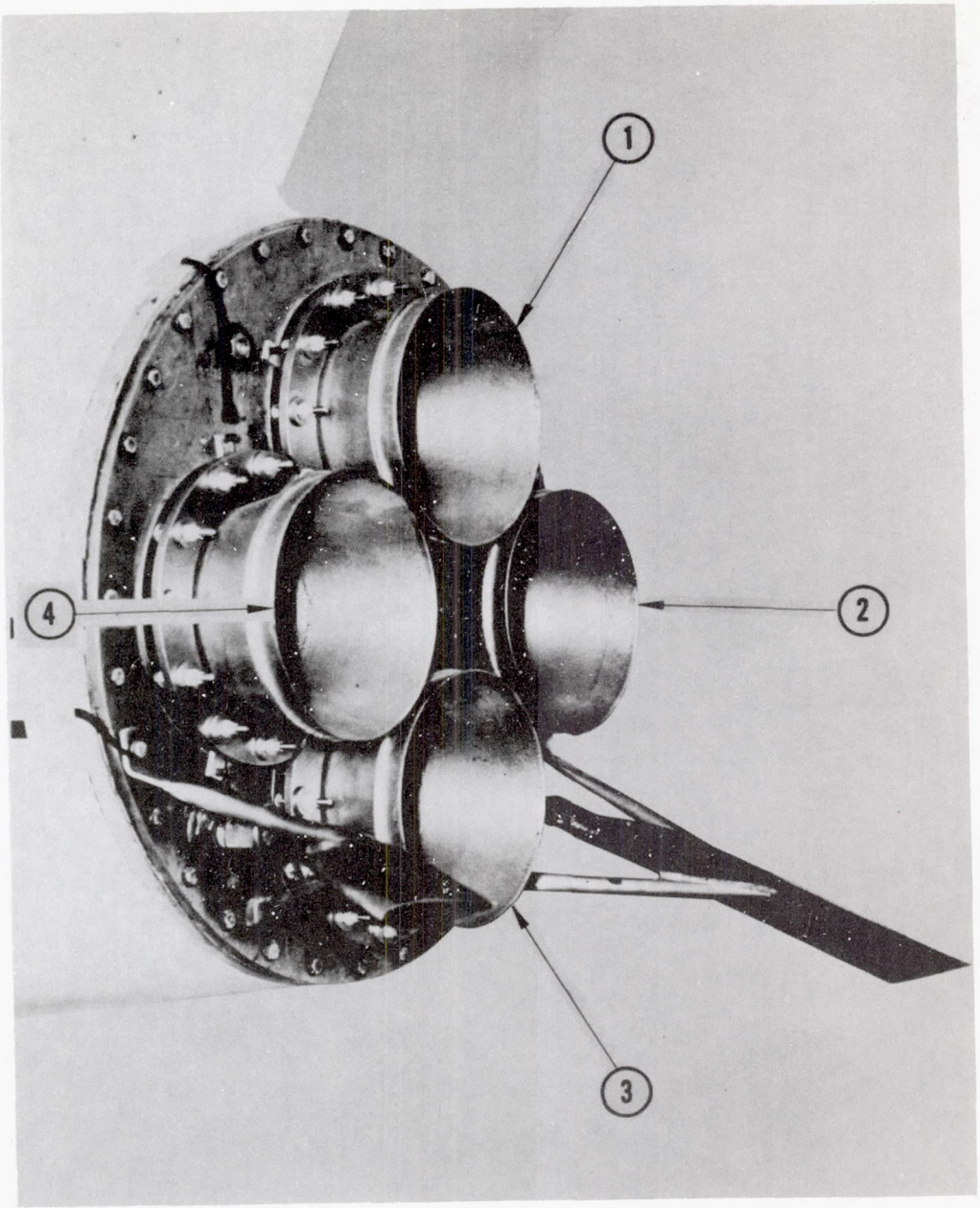


Figure 1.- Three-view drawing of the Douglas D-558-II research airplane.



L-57-1630

Figure 2.- Photograph of the Douglas D-558-II research airplane without nozzle extensions.



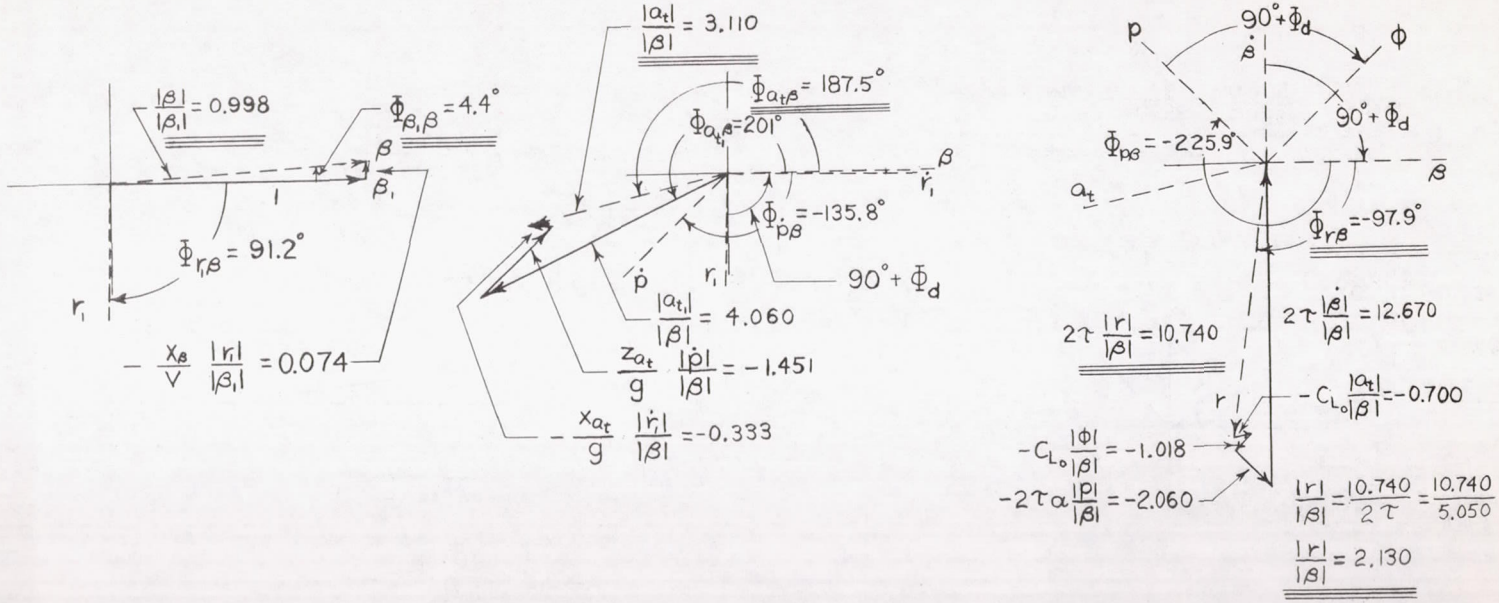
E-1026

Figure 3.- Photograph of the nozzle extensions on the Douglas D-558-II all-rocket research airplane.

$$\frac{|\beta|}{|\beta_1|} = 1 - \frac{X_\beta}{V}\cdot\frac{|\dot{r}_1|}{|\beta_1|}$$

$$\frac{|a_t|}{|\beta|} = \frac{|a_{t_1}|}{|\beta|} + \frac{Z_{a_t}}{g}\cdot\frac{|\dot{p}|}{|\beta|} - \frac{X_{a_t}}{g}\cdot\frac{|\dot{r}_1|}{|\beta|}$$

$$2\tau\frac{|\dot{\beta}|}{|\beta|} + 2\tau\frac{|r|}{|\beta|} - 2\tau\alpha\frac{|p|}{|\beta|} - C_{L_\alpha}\frac{|\phi|}{|\beta|} - C_{L_0}\frac{|a_t|}{|\beta|} = 0$$



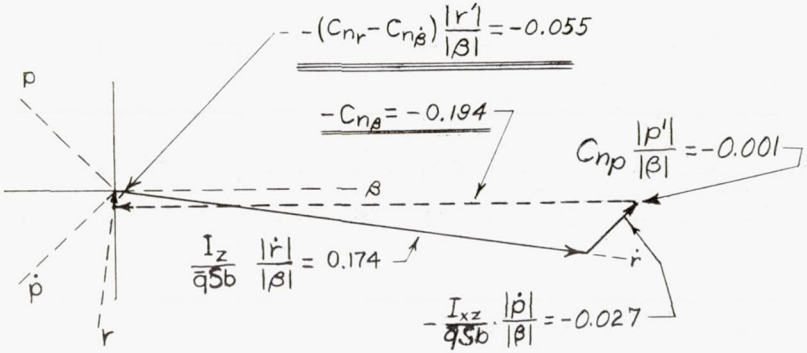
(a) Determination of phase lag and magnification factor of β-vane due to vane location.

(b) Determination of correct value of $\frac{|a_t|}{|\beta|}$. Correction necessitated by lateral accelerometer location.

(c) Determination of $\frac{|r|}{|\beta|}$ and $\Phi_{r\beta}$.

Figure 4.- Typical sequence employed in the determination of lateral derivatives using flight data and the time vector.

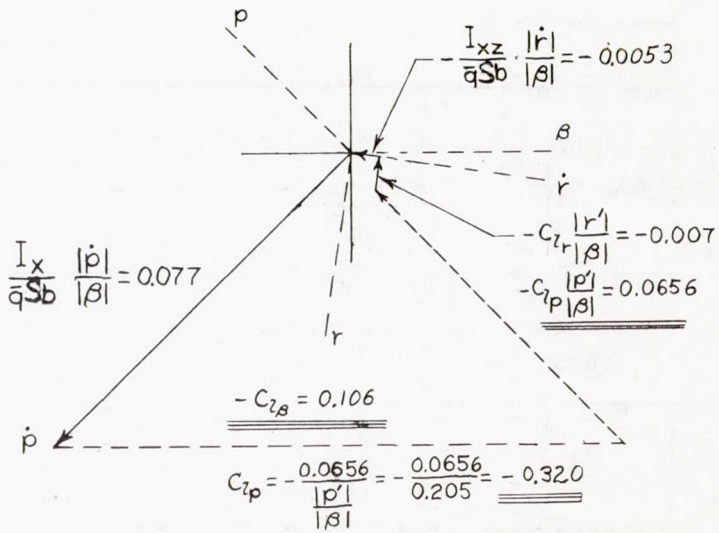
$$\frac{I_z}{\bar{q}Sb}\frac{|\dot{r}|}{|\beta|} - \frac{I_{xz}}{\bar{q}Sb}\frac{|\dot{p}|}{|\beta|} - C_{n_p}\frac{|p'|}{|\beta|} - C_{n_\beta} - (C_{n_r} - C_{n_{\dot{\beta}}})\frac{|r'|}{|\beta|} = 0$$



$$C_{n_r} - C_{n_{\dot{\beta}}} = -\frac{-0.055}{\frac{|r'|}{|\beta|}} = +0.146$$

(d) Determination of C_{n_β} and $\left(C_{n_r} - C_{n_{\dot{\beta}}}\right)$.

$$\frac{I_x}{\bar{q}Sb}\frac{|\dot{p}|}{|\beta|} - \frac{I_{xz}}{\bar{q}Sb}\frac{|\dot{r}|}{|\beta|} - C_{l_r}\frac{|r'|}{|\beta|} - C_{l_\beta} - C_{l_p}\frac{|p'|}{|\beta|} = 0$$



(e) Determination of C_{l_β} and C_{l_p}.

Figure 4.- Concluded.

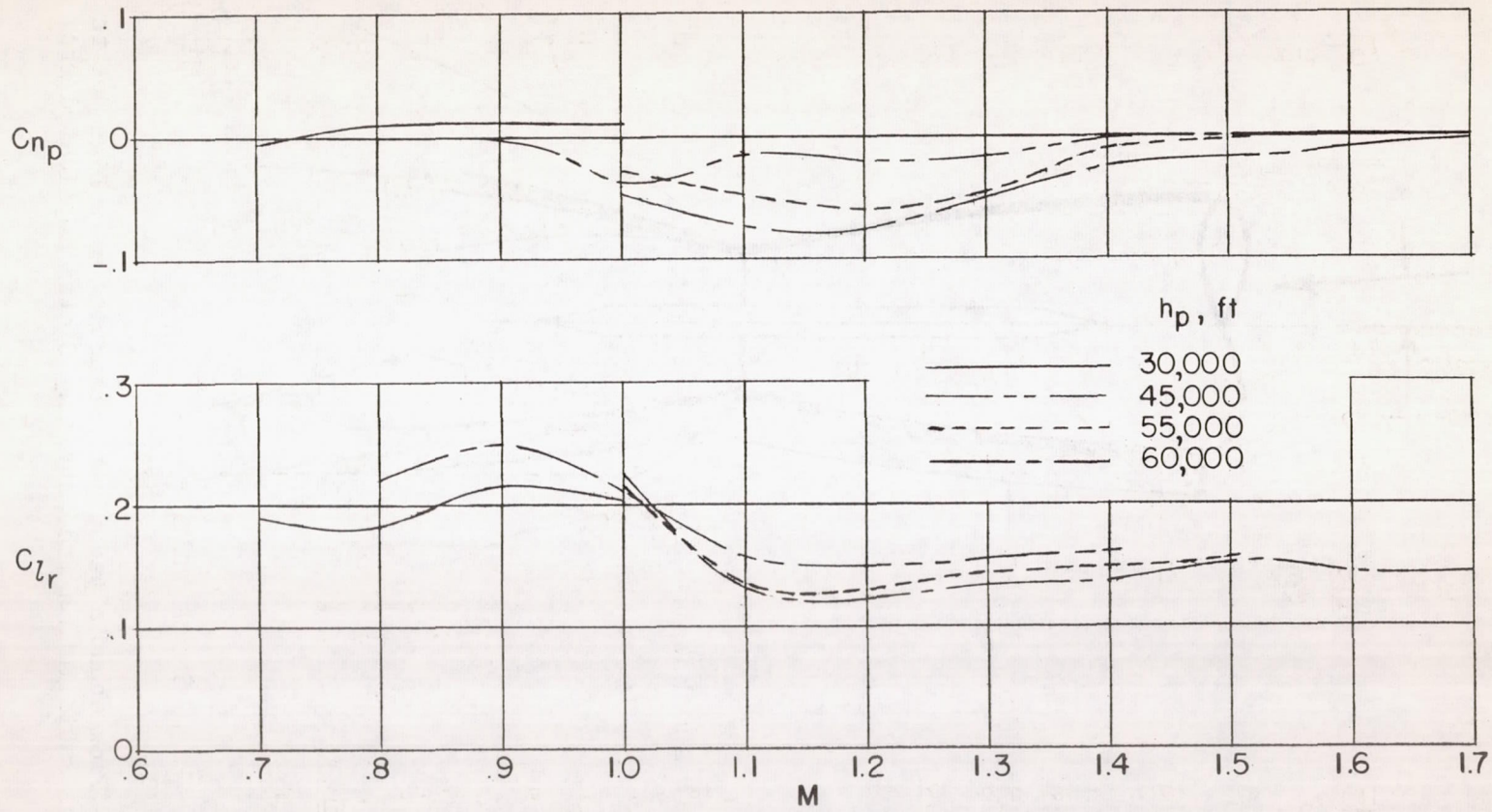


Figure 5.- Calculated values of C_{n_p} and C_{l_r} as functions of Mach number and altitude.

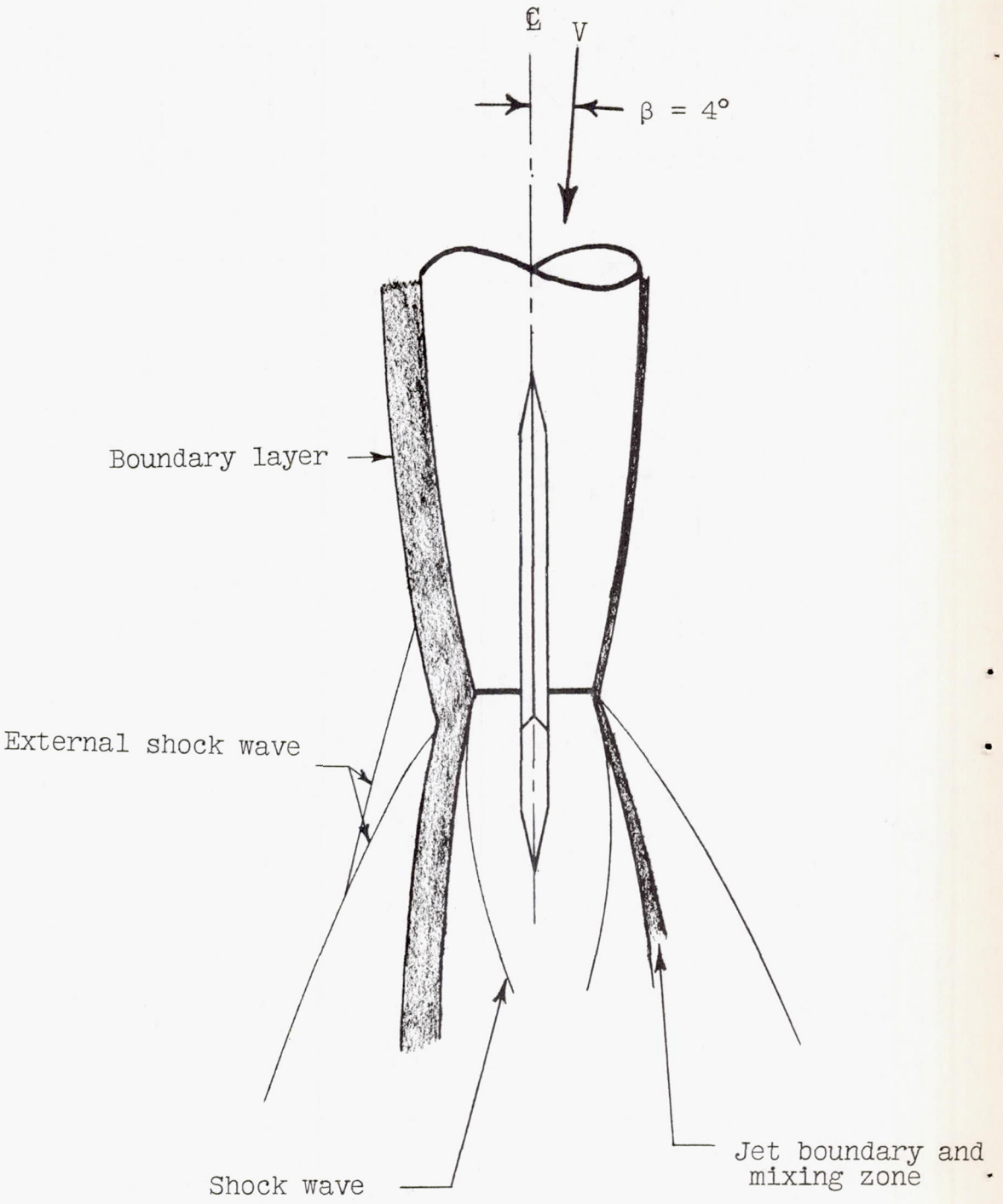
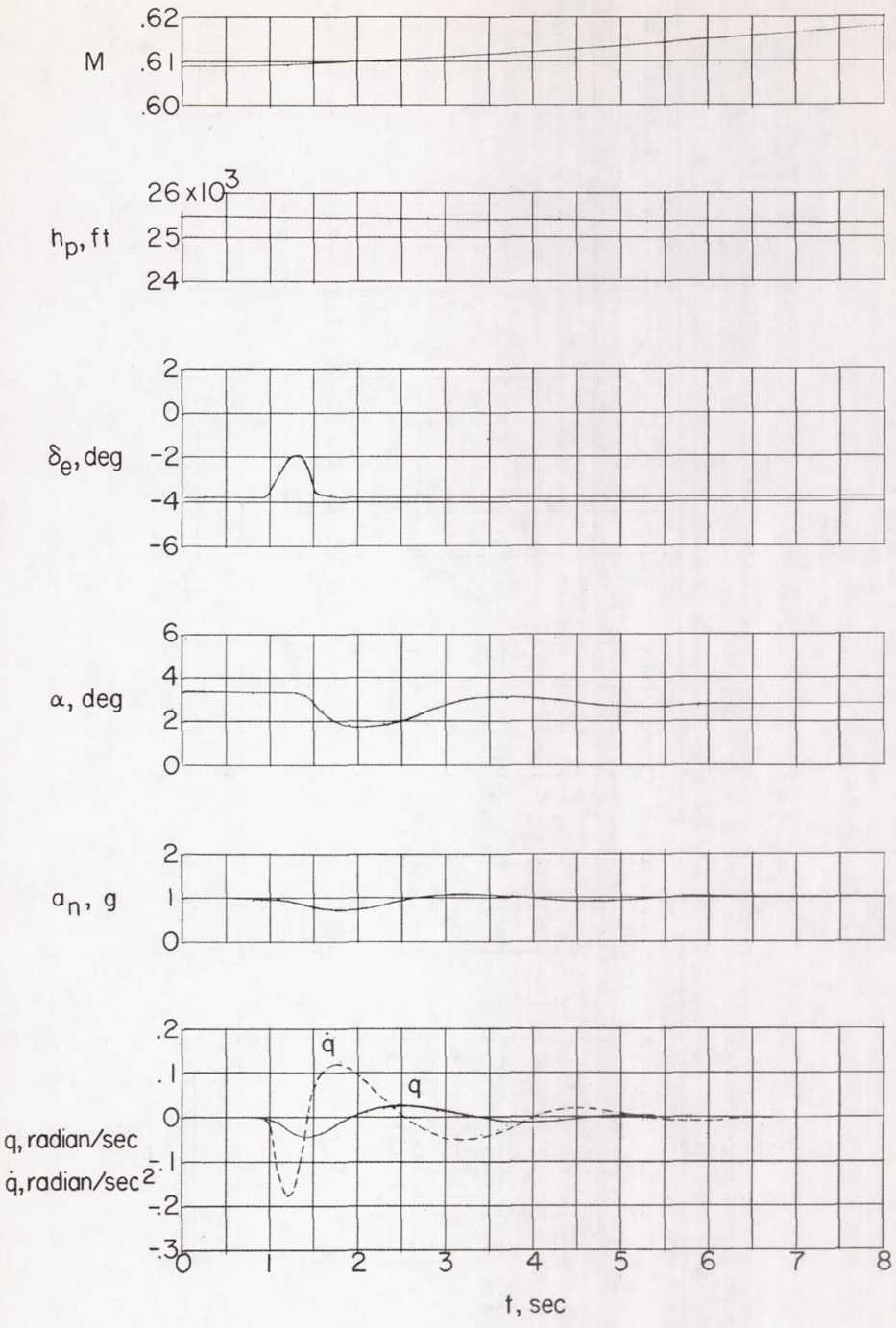
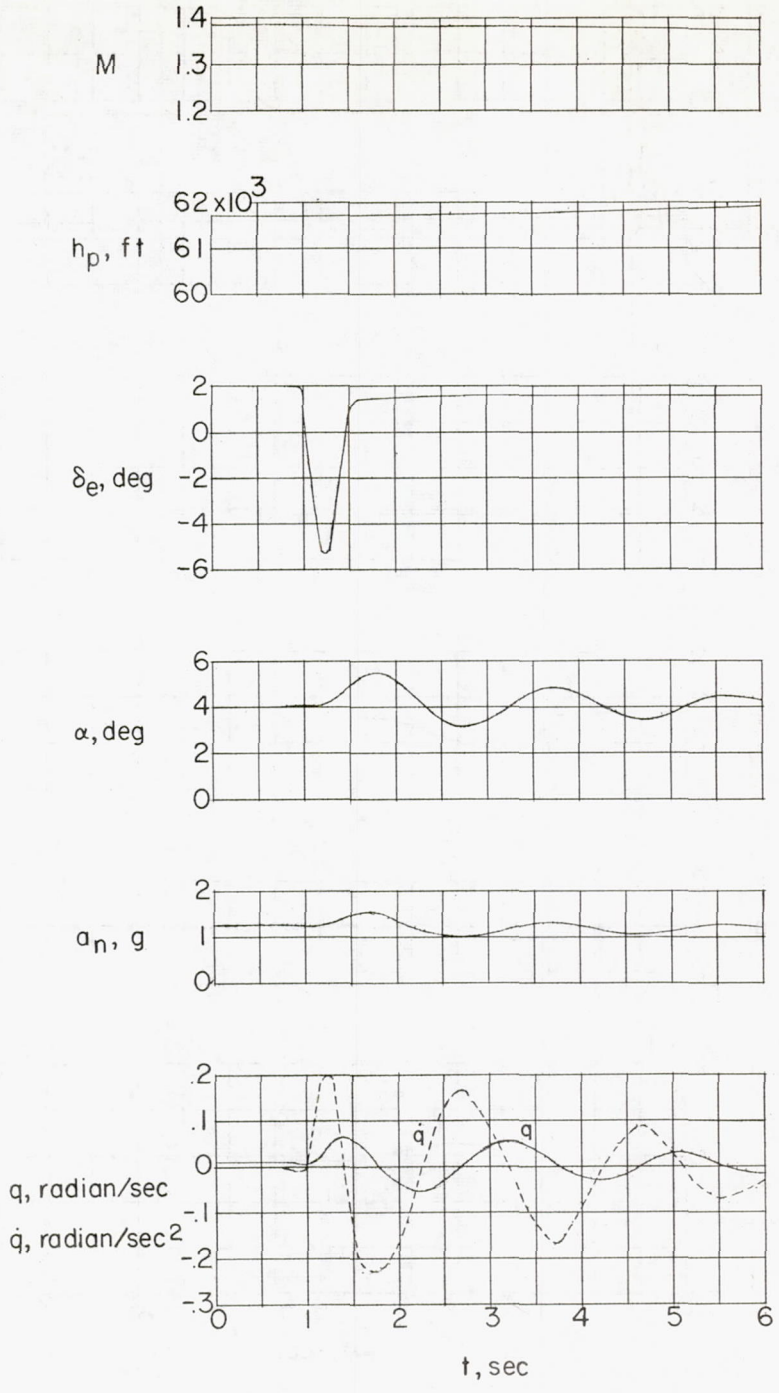


Figure 6.- Flow about a yawed jet exhausting at a high jet-to-stream pressure ratio into a free stream. Sketch duplicated from reference 2.



(a) Rocket and jet airplane; M = 0.61; h_p = 25,400 ft.

Figure 7.- Time histories of longitudinal oscillations induced by an elevator pulse.



(b) All-rocket airplane; M = 1.38; h_p = 61,700 ft.

Figure 7.- Concluded.

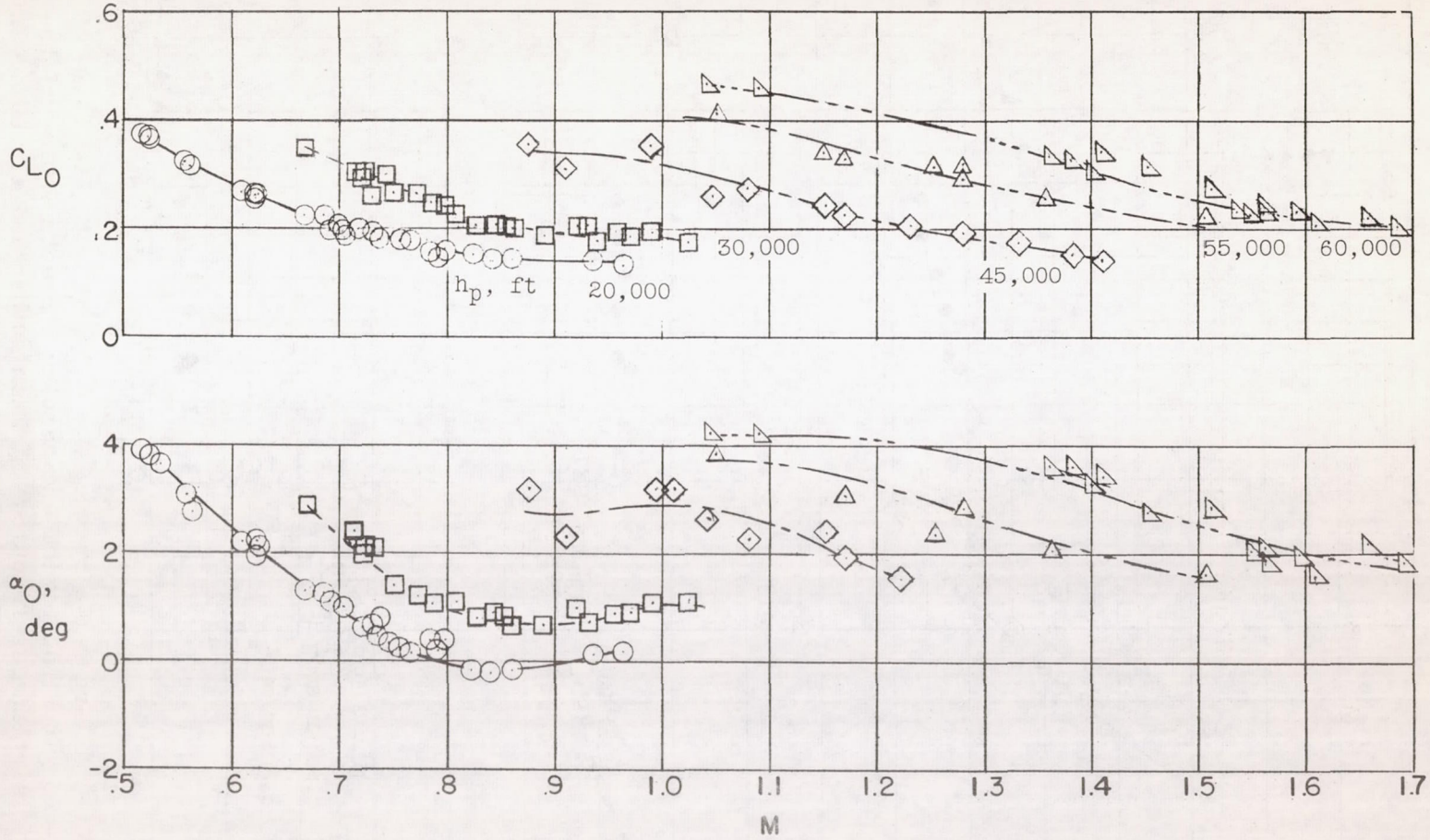


Figure 8.- Variation of 1 g lift coefficient and corresponding trim angle of attack with Mach number.

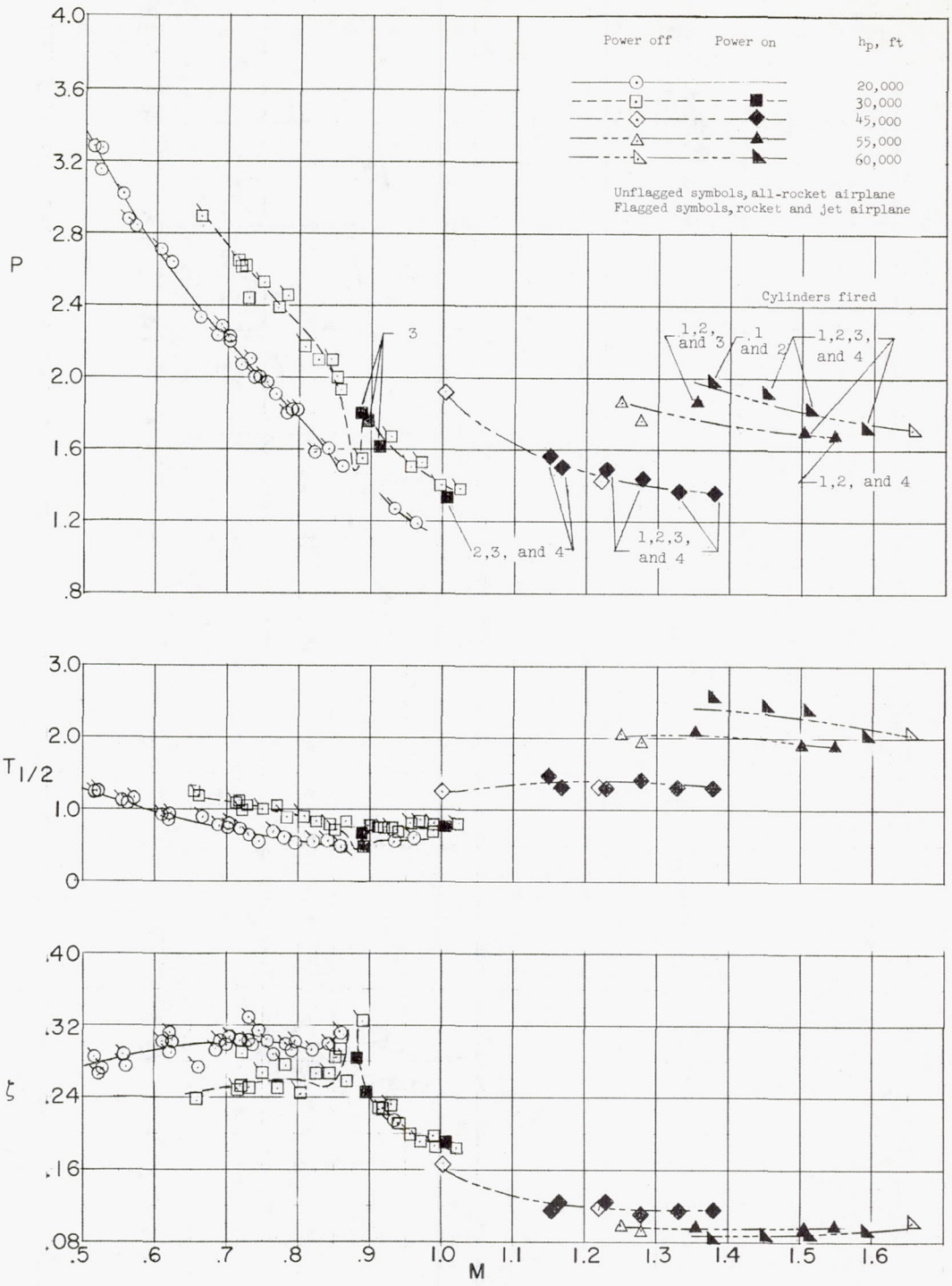


Figure 9.- Longitudinal period and damping characteristics of the D-558-II airplane as functions of Mach number and altitude.

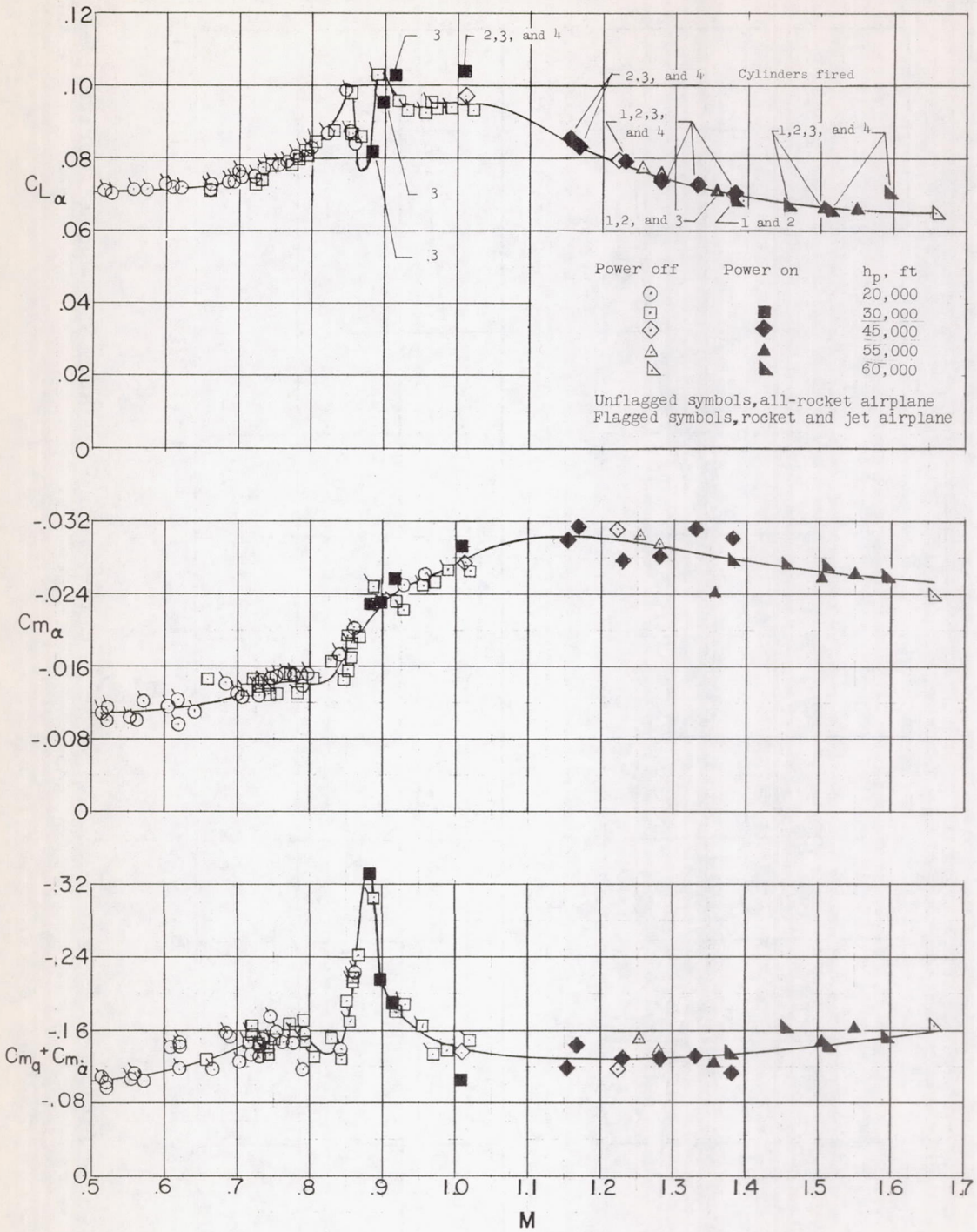


Figure 10.- Variation of static and dynamic longitudinal stability derivatives of the D-558-II airplane with Mach number.

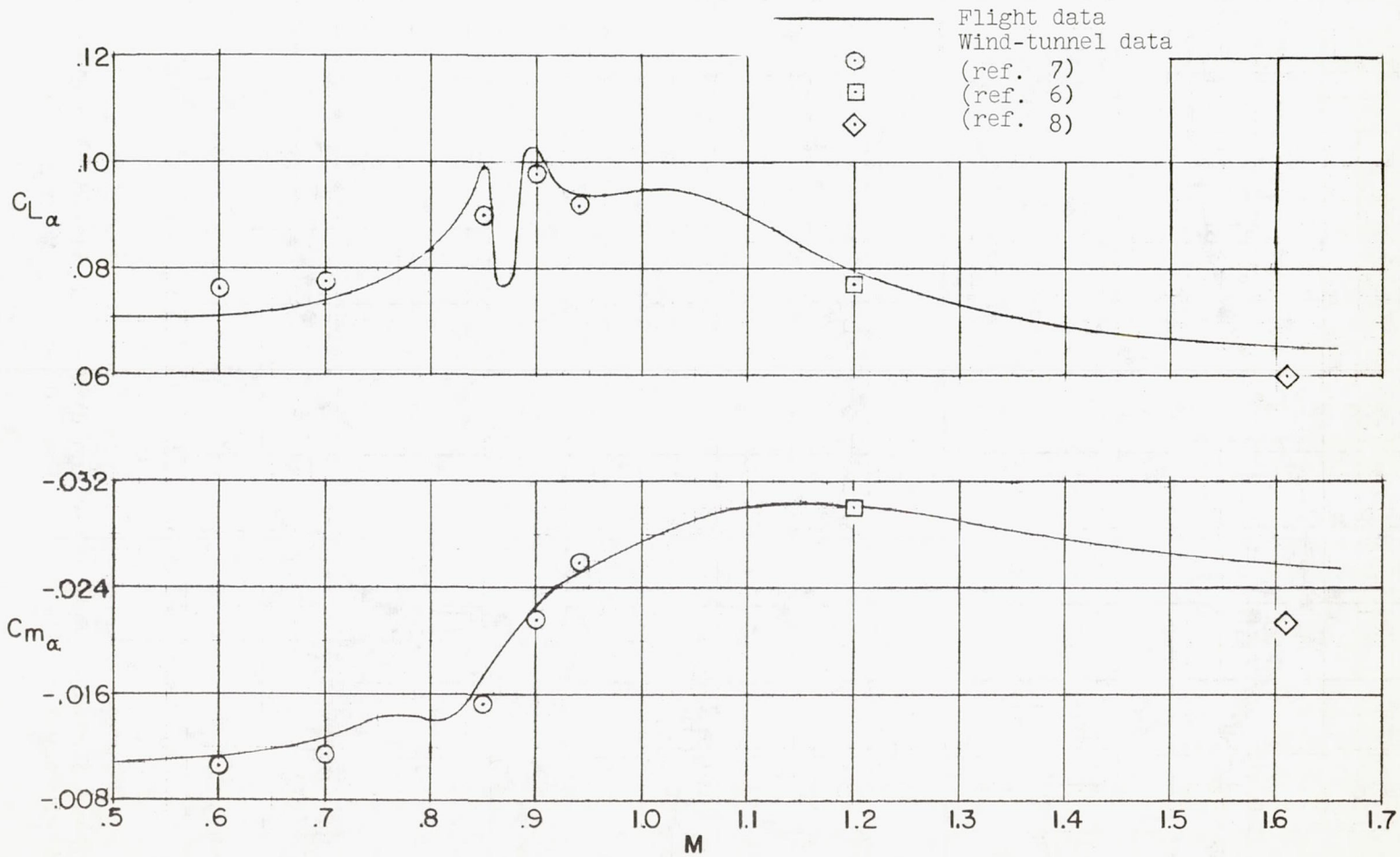
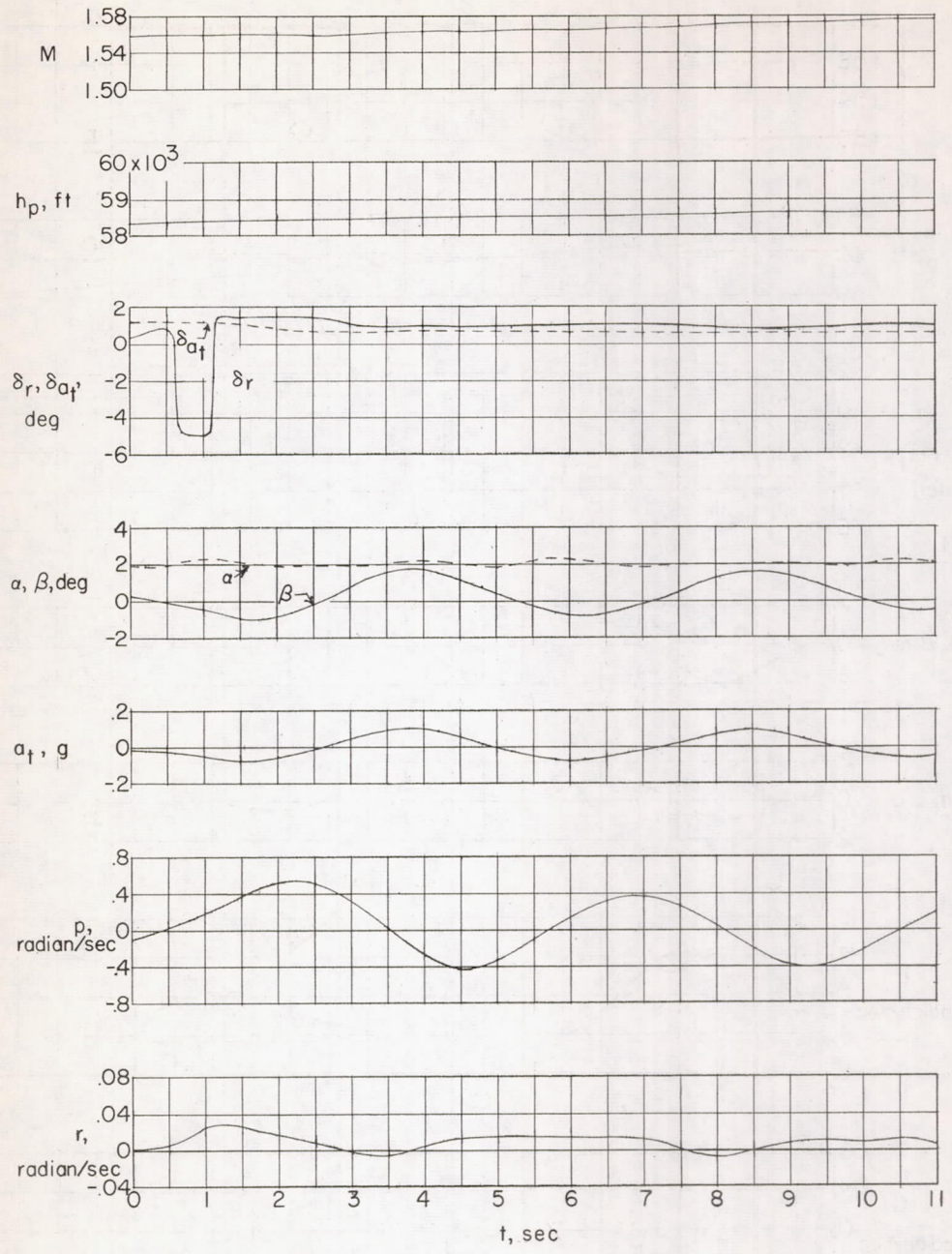
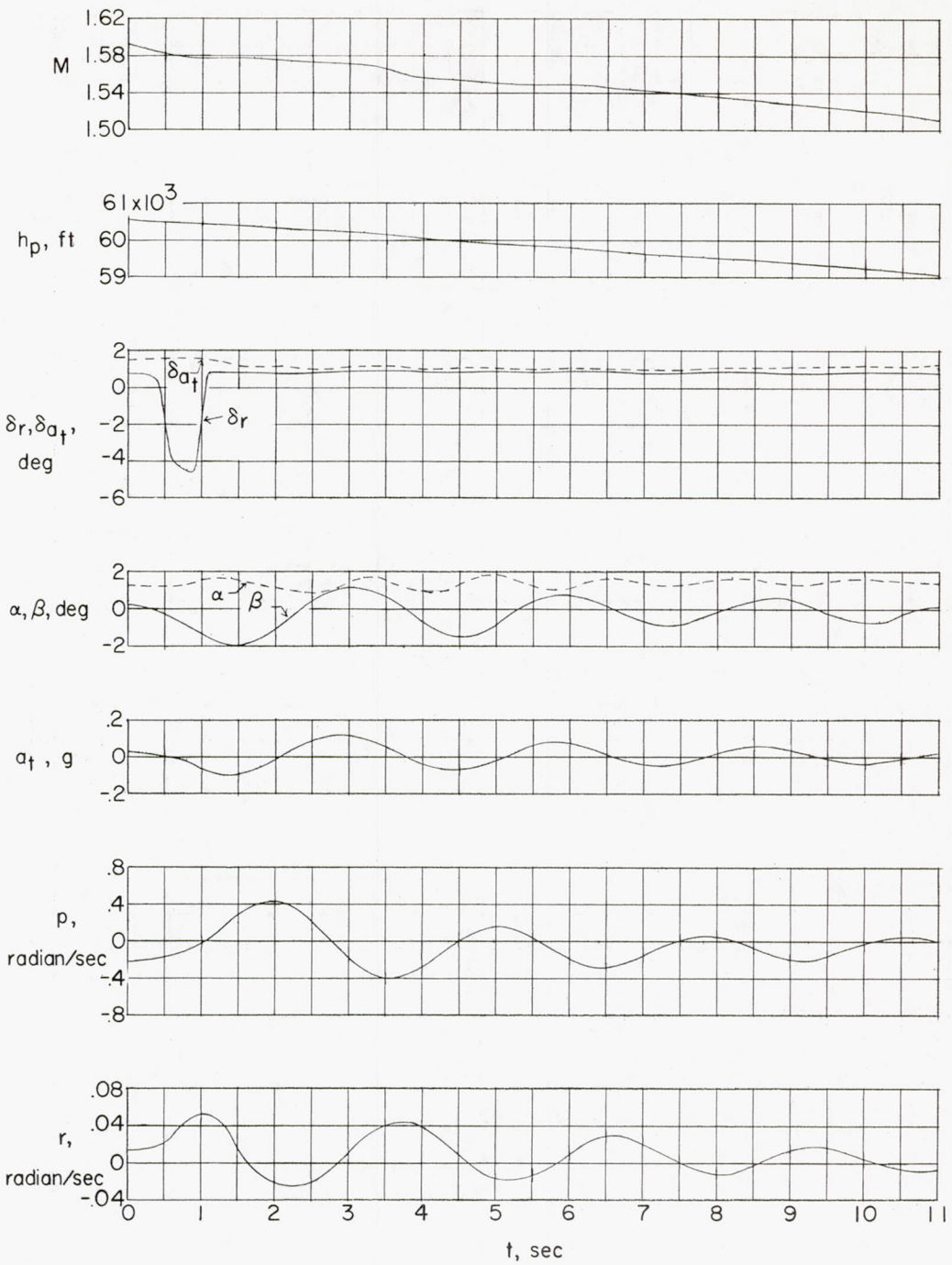


Figure 11.- Comparison of longitudinal flight derivatives with available wind-tunnel derivatives for power on and power off.



(a) Power on, cylinders 1, 2, and 4 firing.

Figure 12.- Time histories of lateral oscillations of the all-rocket airplane. Rudder held against slotted stop during transient oscillations.



(b) Power off.

Figure 12.- Concluded.

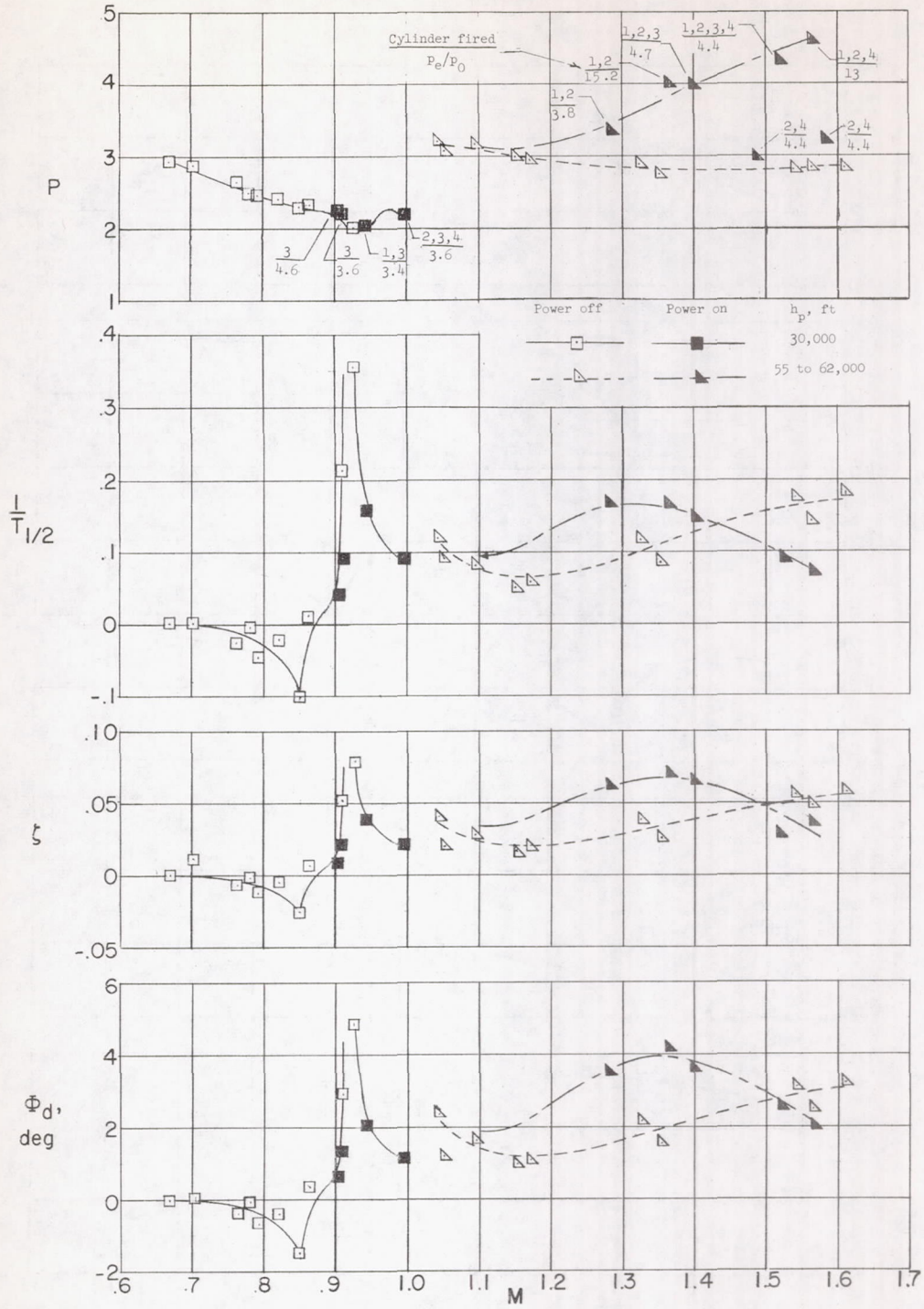


Figure 13.- Influence of power on the variation of lateral period and damping with Mach number. Control surfaces fixed.

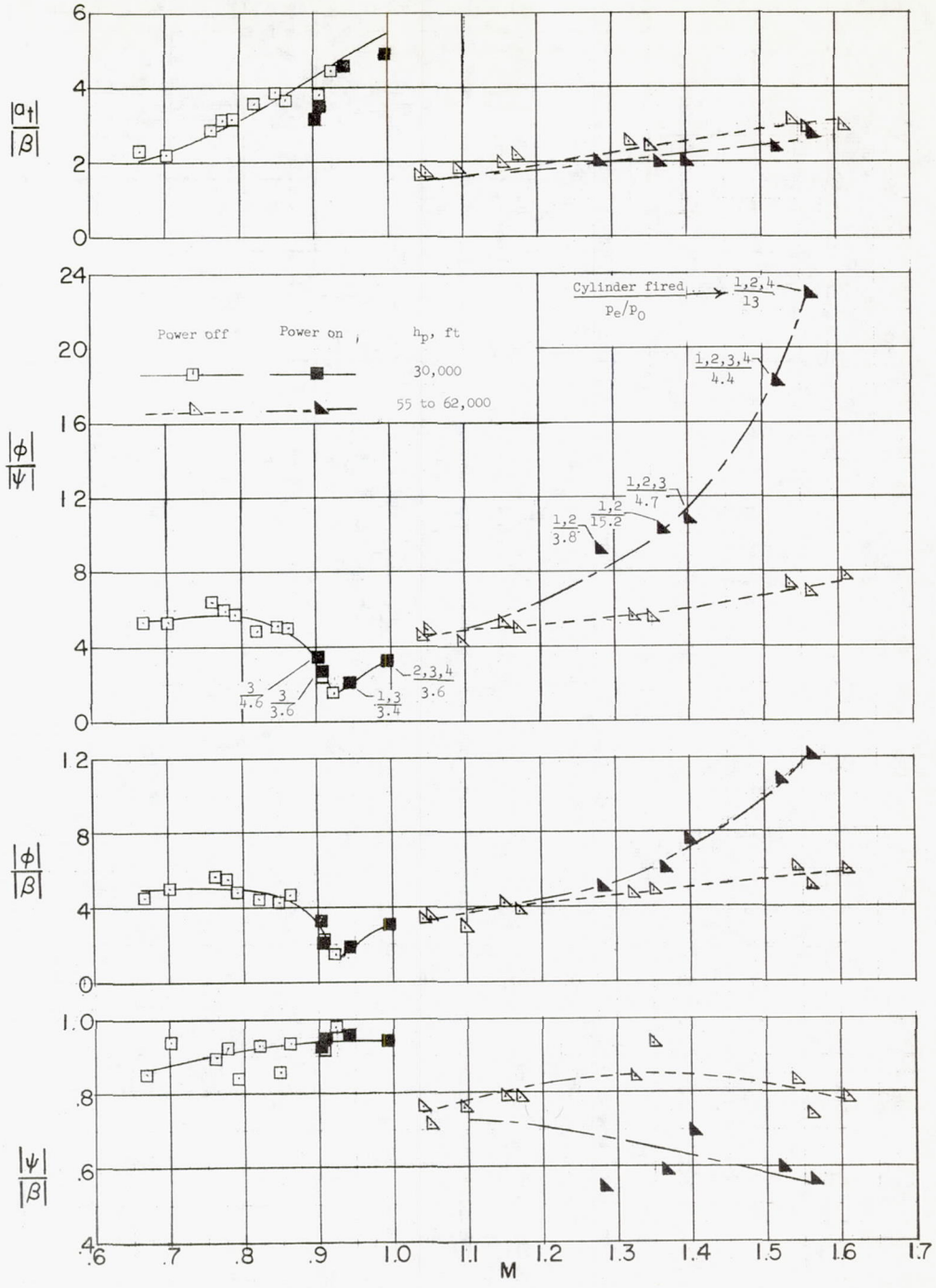


Figure 14.- Influence of power on the variation of lateral amplitude ratios with Mach number. All-rocket airplane. Control surfaces fixed.

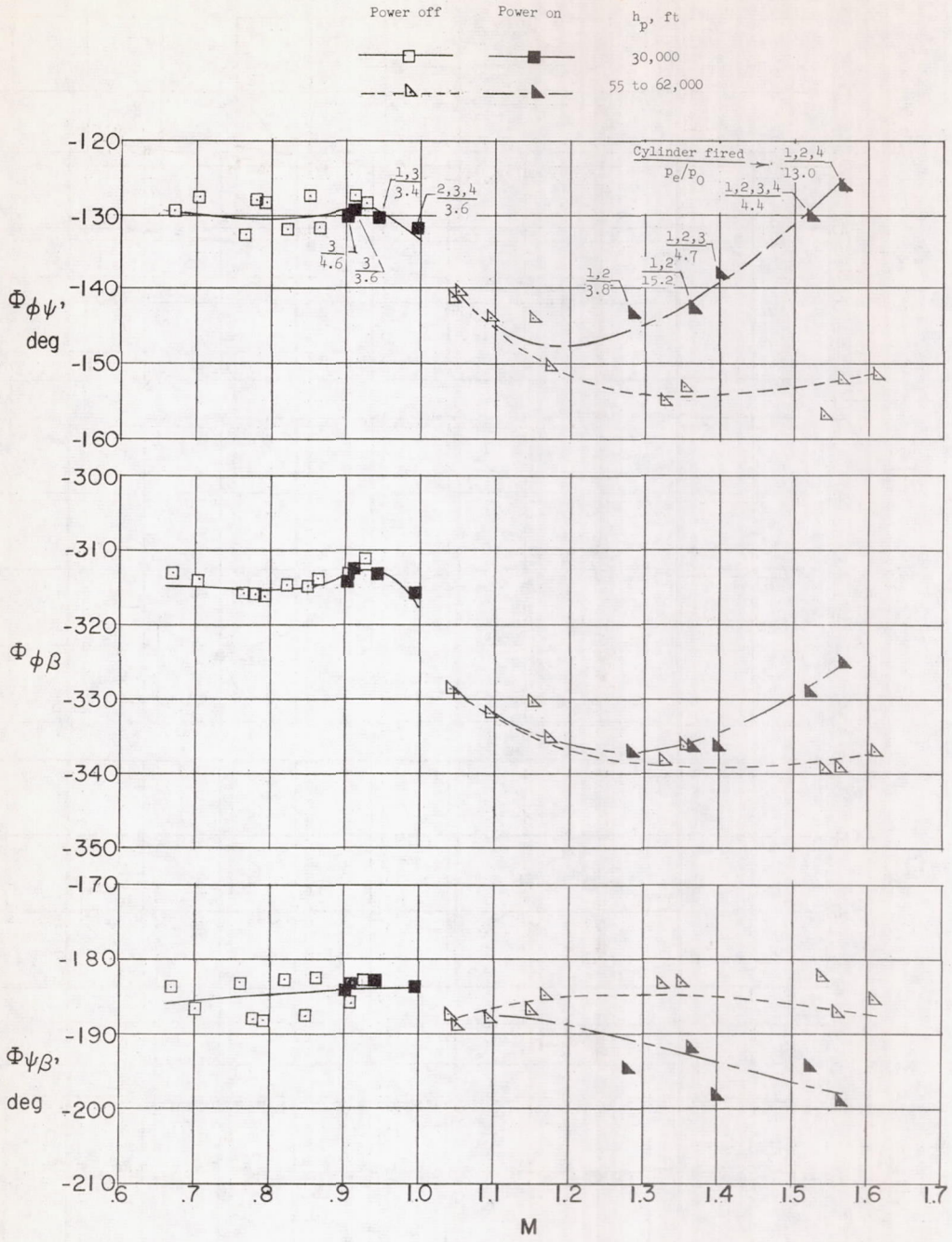


Figure 15.- Influence of power on the variation of lateral phase angles with Mach number. All-rocket airplane.

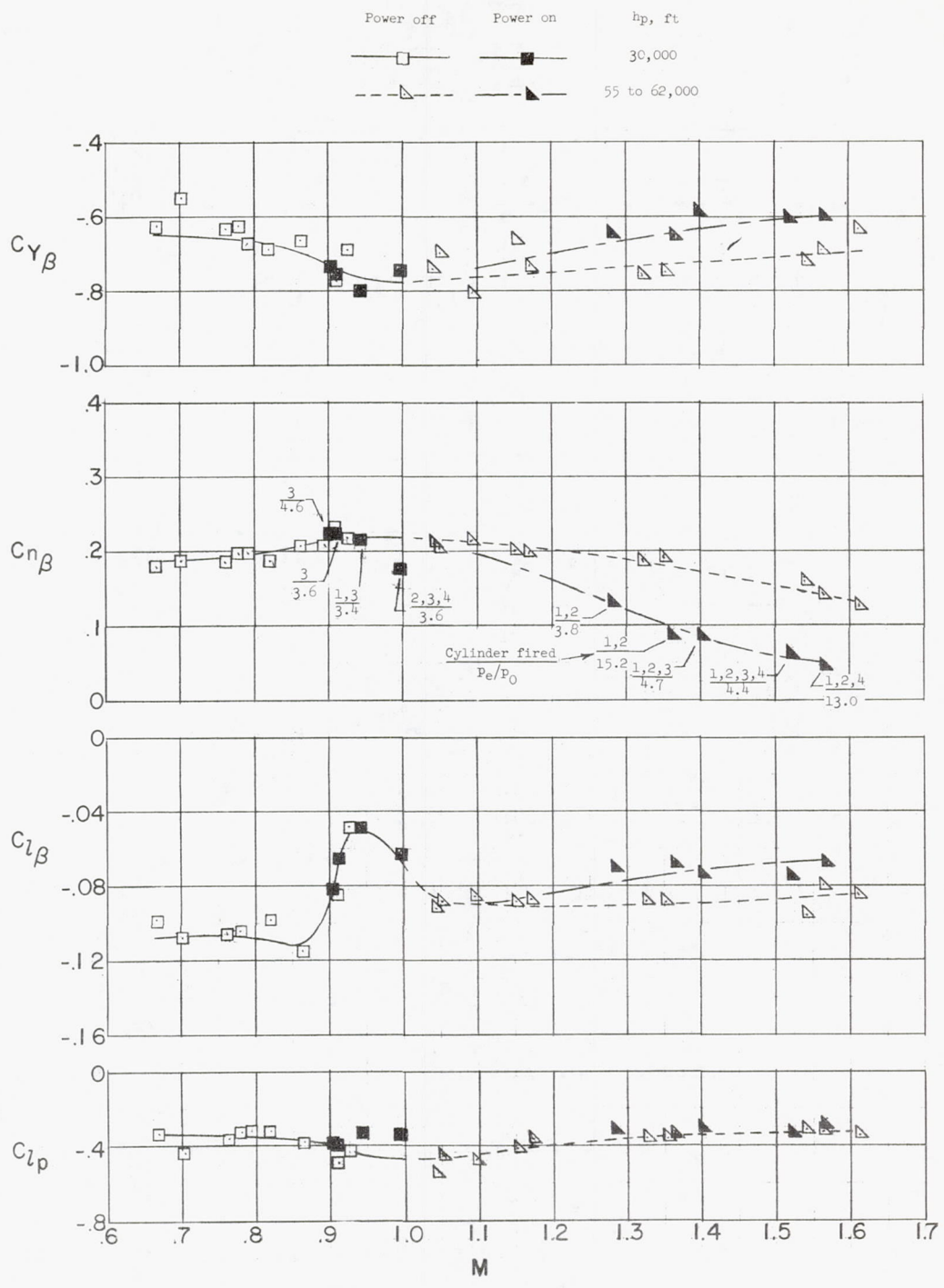


Figure 16.- Influence of power on the variation of static and dynamic lateral stability derivatives with Mach number. Control surfaces fixed.

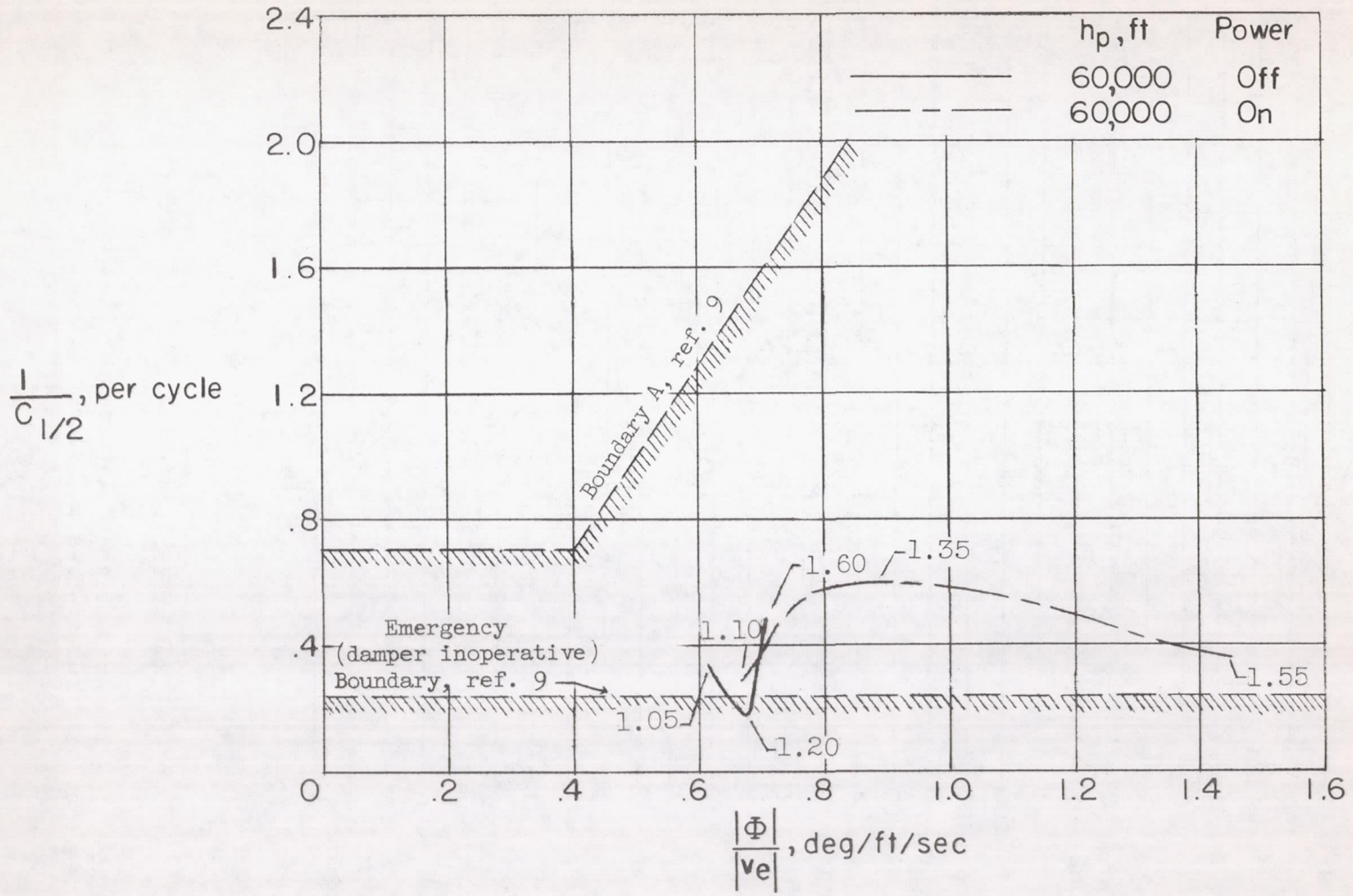
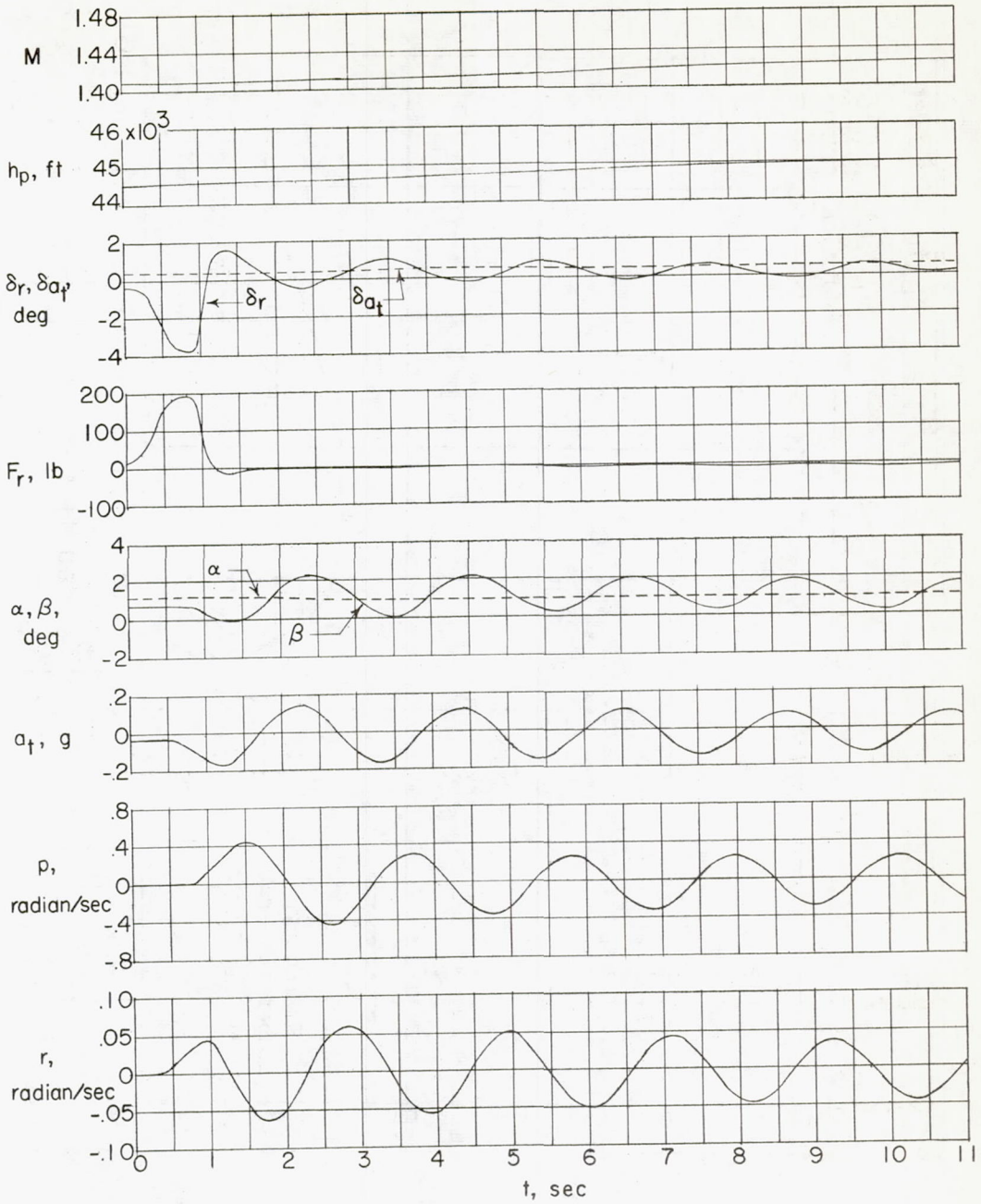
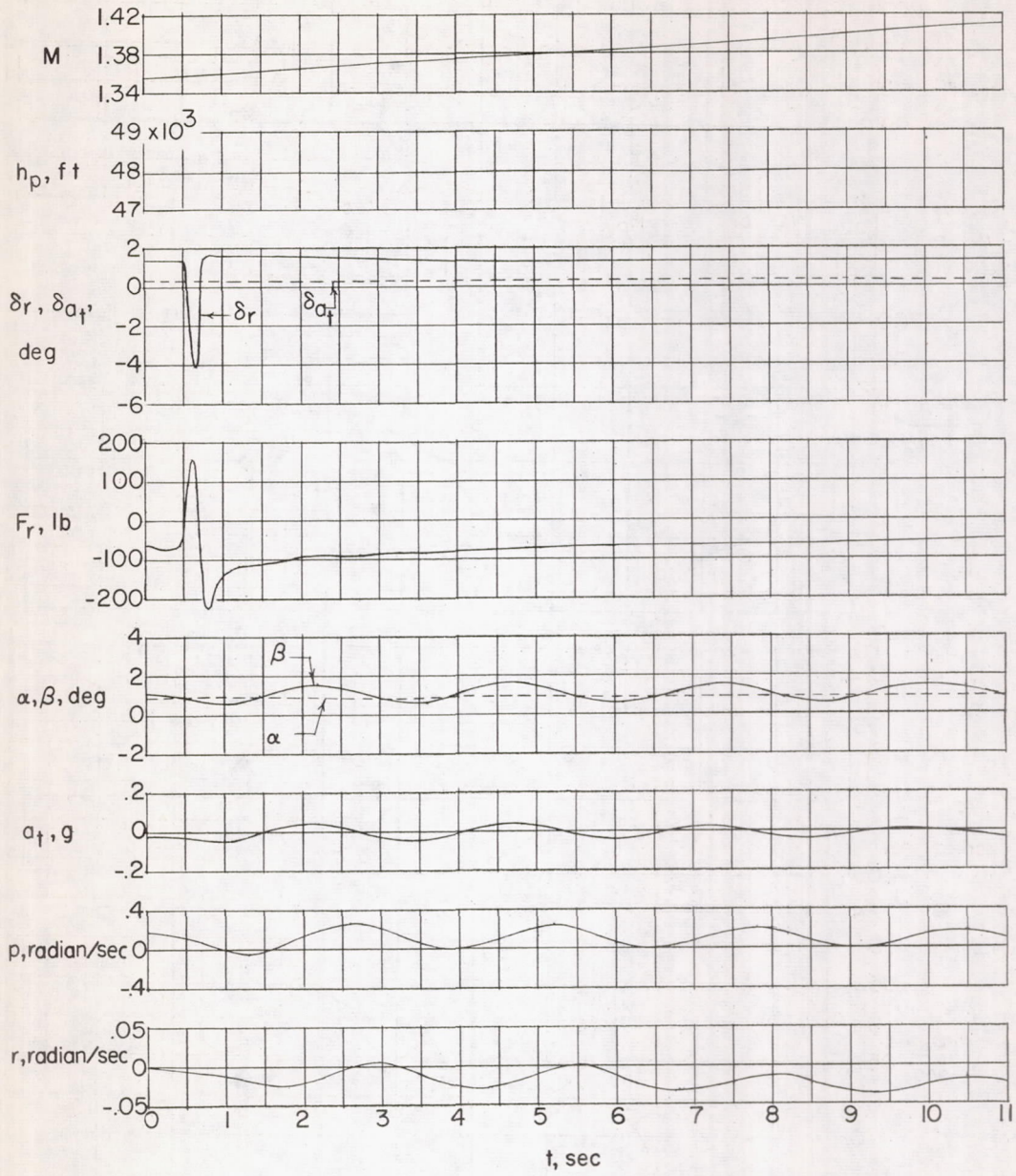


Figure 17.- Comparison of supersonic lateral oscillatory characteristics of the all-rocket airplane for power-on and power-off conditions with lateral damping criteria of reference 9.



(a) Rudder free; M = 1.41; h_p = 44,500 ft.

Figure 18.- Time histories of lateral oscillations of the all-rocket airplane for rudder-free and rudder-fixed conditions. All four rocket cylinders firing.



(b) Rudder fixed; M = 1.38; h_p = 48,000 ft.

Figure 18.- Concluded.

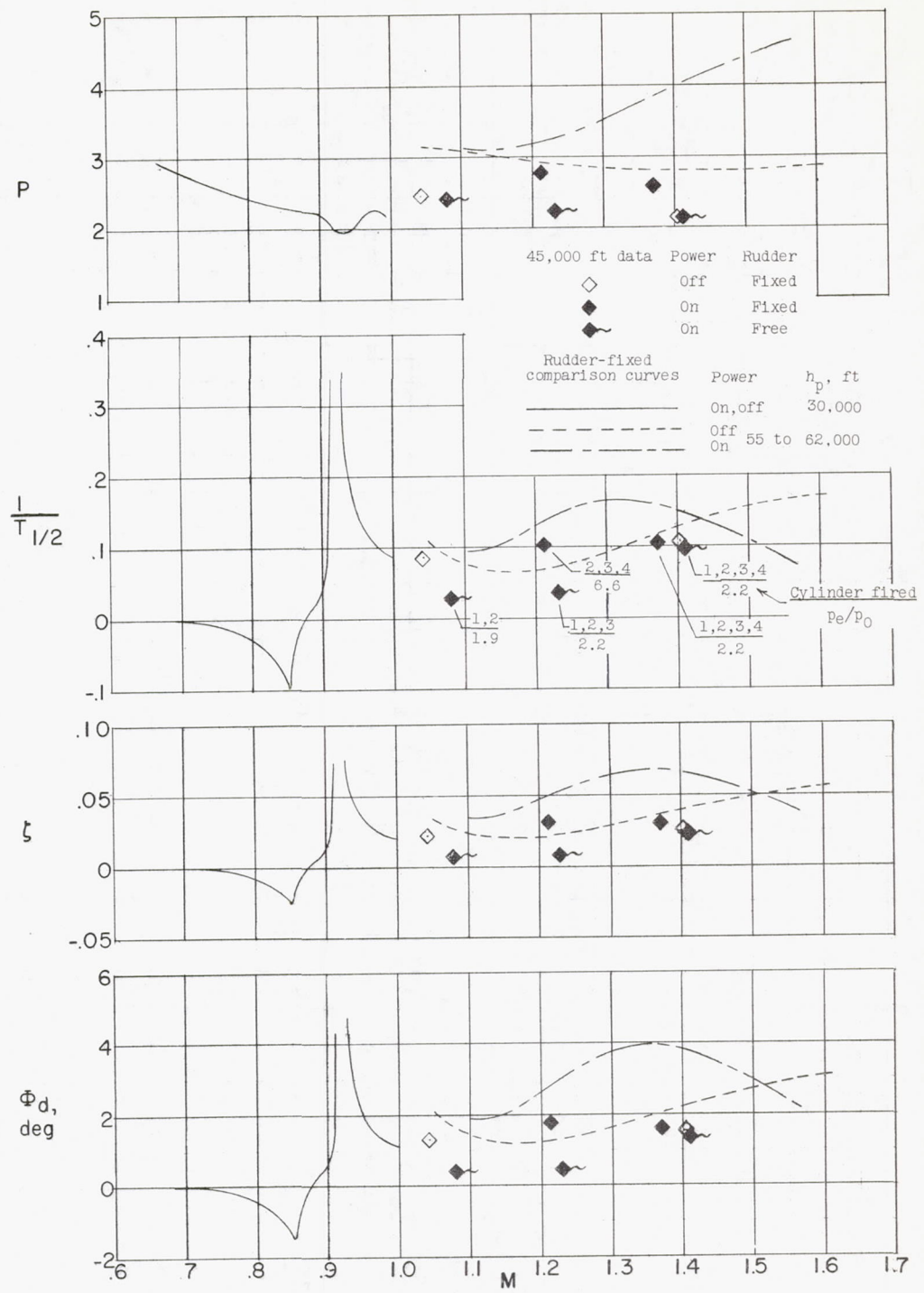


Figure 19.- Influence of free rudder during powered flight on the lateral period and damping of the all-rocket airplane.

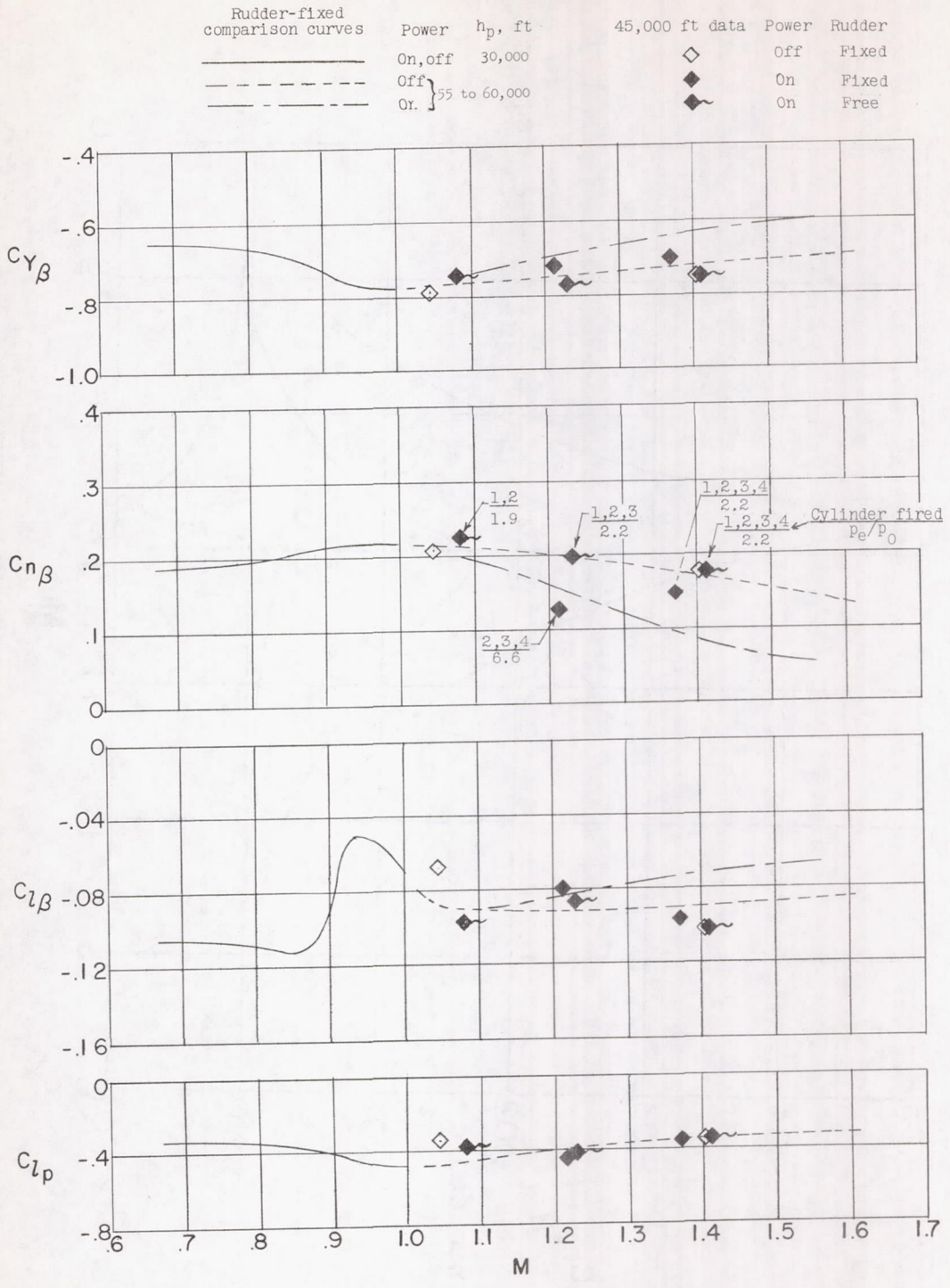


Figure 20.- Influence of free rudder during powered flight on the static and dynamic lateral stability derivatives.

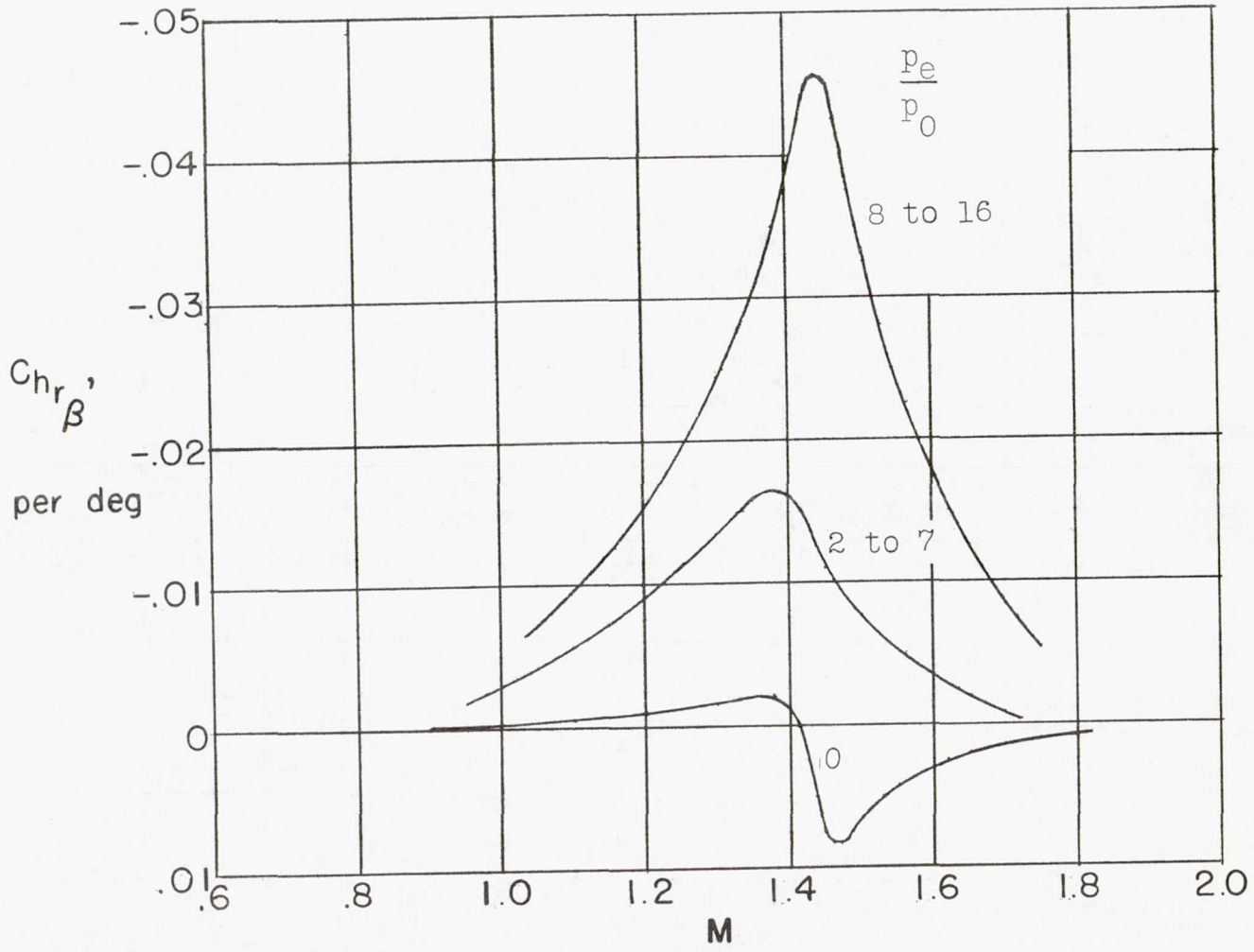
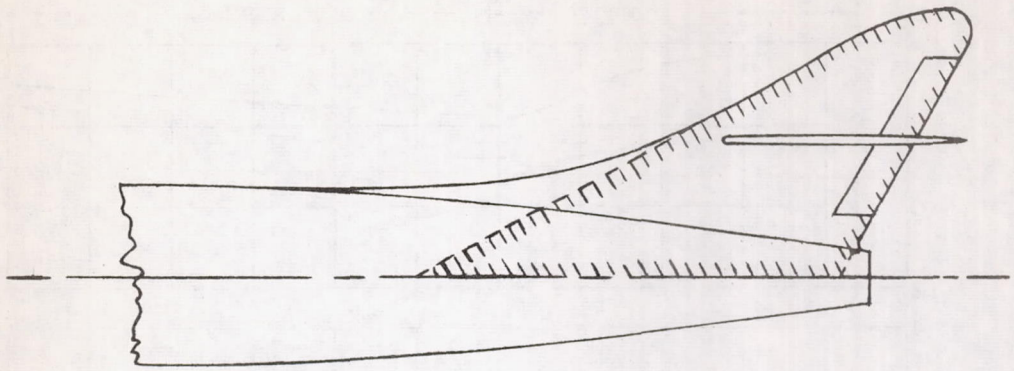
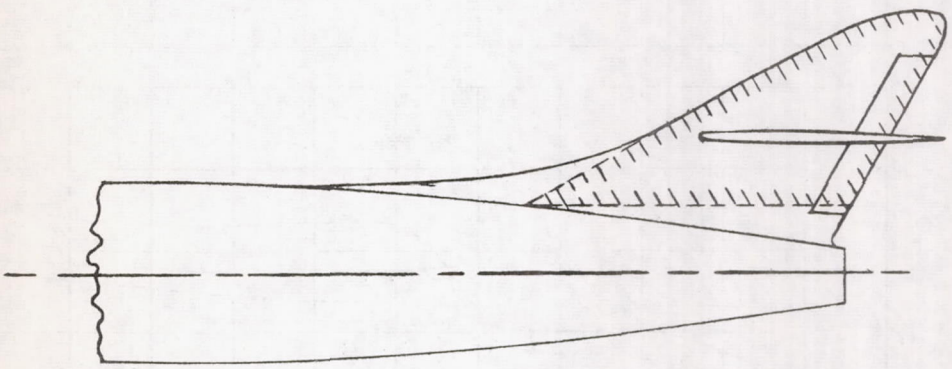


Figure 21.- Approximate variation of rudder hinge-moment parameter with Mach number at different pressure ratios (reproduced from ref. 1).



Area = 56.6 sq ft

(a) Subsonic calculations.



Area = 36.6 sq ft

(b) Supersonic calculations.

Figure 22.- Vertical-tail-surface areas used in estimating values of calculated derivatives. Power off.

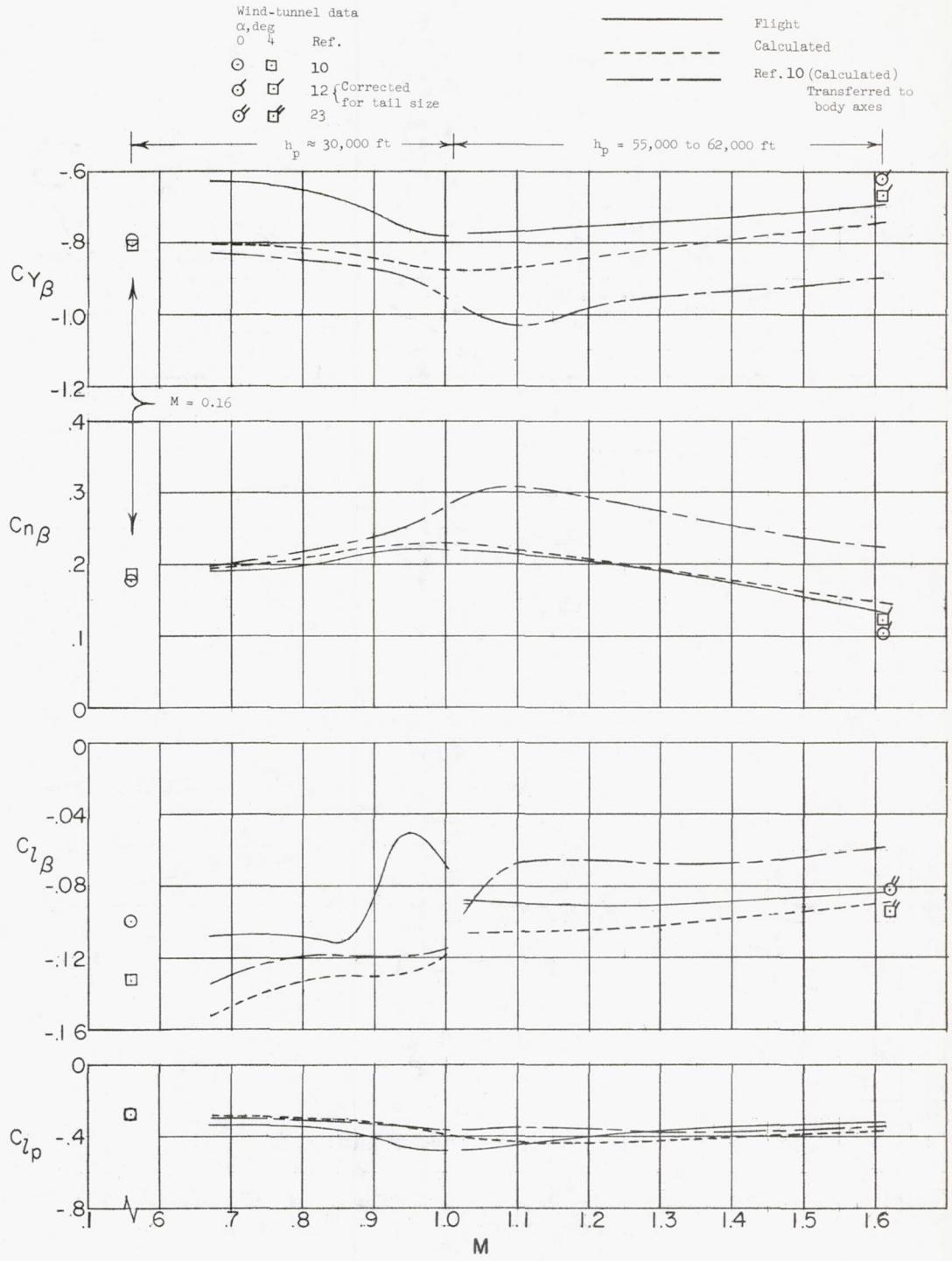


Figure 23.- Comparison of lateral flight derivatives with calculated and available wind-tunnel derivatives for power-off conditions. Body axes.